Measured Sun Noise Temperatures at 32 Gigahertz

T. Y. Otoshi[1]

Sun experiments were performed to develop methods for accurately mapping the Sun noise temperatures over the entire solar disk at 32 GHz (Ka-band). High-resolution mapping of the Sun's noise temperatures was obtained through the use of the 34-m beam-waveguide (BWG) antenna and the Ka-band monopulse receiving system at DSS 13. Detailed mapping of the solar disk was possible because at 32 GHz the BWG antenna has a full 3-dB beamwidth that is only 17 mdeg compared to the angular Sun diameter of about 0.5 deg. Due to the expected high noise temperature of the Sun (>10,000 K), methods had to be developed so that the incoming Sun noise-temperature power would not saturate the antenna receiving system. Of several methods investigated, only the absorber and waveguide attenuator methods were considered (1) to be easy and inexpensive to implement into any existing BWG receiving system and (2) to have the potential of giving accurate results. Both of these methods were used to measure the Sun noise temperatures presented in this article.

Due to the high solar activity during the experiments, it was not possible to obtain repeatable results on different days and even on the same day. However, useful information has been obtained about the Sun's noise-temperature characteristics during the period of maximum solar activity that occurred in the year 2000. To this author's knowledge, this is the first time that a large (34-m) antenna was used to map the Sun's noise-temperature profile over its entire surface at 32 GHz.

I. Introduction

The purpose of the Sun Experiment Task was to develop a simple and inexpensive method for measuring the Sun's noise temperature at 32 GHz with the use of Deep Space Network (DSN) 34-m antennas. It was required that new methods be developed to prevent receiver saturation caused by the strong incoming Sun's noise power. This task is important for increasing the accuracy of measuring system noise temperatures when tracking a spacecraft in the vicinity of the Sun at Ka-band. In addition, if a method is developed that overcomes the receiver saturation problem, it might be possible to employ raster scan techniques to quantify scattering from the antenna's tripod struts as functions of the Sun's position.

Previous work has been done by JPL experimenters on noise-temperature measurements looking directly at the Sun or in the vicinity of the Sun [2–4]. The 34-m BWG antenna system noise temperatures

[1] Communications Ground Systems Section.

The research described in this publication was carried out by the Jet Propulsion Laboratory, California Institute of Technology, under a contract with the National Aeronautics and Space Administration.

are currently calibrated through the use of an ambient load thermal noise standard and the zero point of a power meter located in the DSS-13 control room. Injected noise diode pulses of about 20 K are used to determine receiving system linearity. System noise-temperature calibrations are valid only up to the system temperature (or T_{op}) value measured when the ambient load is connected to the input of the low-noise amplifier (LNA). For the Ka-band monopulse receiving system at DSS 13, the upper limit of valid system noise-temperature calibration is about 350 K. Linearity of the receiving system is also not calibrated above this upper limit point. Without running special tests, the saturation point above 350 K is not known.

The Sun's noise temperature during the quiet Sun cycle is about 9960 K at 31.4 GHz [1,2]. When the 34-m antenna points at a quiet Sun and the antenna system has 50 percent efficiency, the measured Sun temperature will be about 5000 K at 32 GHz. This high value is far above the calibrated region of the DSS-13 BWG receiving system. Therefore, a need existed to find a way to measure the Sun's noise temperature accurately at these high levels of 5000 K or more. Although several gain reduction methods were considered for reducing the Sun's noise temperature so that it would be within the calibrated region of the receiver, only two methods, the absorber and waveguide attenuator methods, were extensively investigated.

In Section II, the absorber and waveguide attenuator methods are described. Section III discusses the measurement and data reduction methodology; Section IV presents measured Sun noise temperatures; and Section V gives a summary and recommendations for follow-on work and ways to improve future Sun noise-temperature measurements.

II. Gain Reduction Methods

Table 1 shows seven candidate gain reduction methods that could be used for attenuating the Sun's noise power coming into the antenna receiving system. Most of the methods attenuate the signal before reaching the LNA; another method attenuates the signal in front of the follow-up receiver. It was desired that the Sun's noise power be reduced such that the measured Sun noise temperature would be within the calibrated range of the antenna receiving system after attenuation. Advantages and disadvantages of each method are also shown in Table 1.

The subreflector z-axial defocus method is the simplest but was not used because the 34-m antenna patterns at 32 GHz change significantly as a function of subreflector z-axis defocus position, as shown in Fig. 1. Although this method was not used for the Sun experiment, the subreflector defocus method might be useful for other applications. Far-field patterns, as a function of subreflector defocus positions for the 34-m antennas, were furnished by W. Veruttipong of the Communications Ground Systems Section. These patterns are not known to have been published in any technical reports or books. Hence, these patterns will be presented and documented in this article.

The absorber and waveguide attenuator methods are the last two methods shown in Table 1. For the absorber method, an absorber sheet is used to attenuate the incoming Sun's noise power in front of the LNA so as not to saturate the LNA. For the waveguide attenuator method, a waveguide variable attenuator is used to attenuate the Sun's noise power going into the follow-up receiver. For this method, it is assumed that the Sun's noise power does not saturate the LNA but instead saturates the follow-up receiver. The absorber and waveguide attenuator methods were extensively investigated because (1) they were easy and inexpensive to implement and (2) they had the potential of giving the most accurate results. Both methods are discussed in detail in the following.

A. Absorber Method

The absorber method involves laying a flat, thin absorber sheet on top of the Kapton cover on the feed-horn aperture. The main advantage of this method is that the technique can be easily used for any

Table 1. Antenna receiving system gain reduction methods to keep Sun noise temperature from saturating the LNA high-electron mobility transistor (HEMT) and/or the follow-up receiver.

Method	Description	Advantages	Disadvantages	Status/recommendation
1	Use existing 28-dB coupler. Reconfigure path so that 28-dB coupling arm becomes main path.	None.	Difficult to implement. Reconfiguration of 28-dB coupling arm to being main path is the same as installing a 28 pad in front of LNA. Gain is reduced 28 dB but T_{op} increases 300 K.	Did a theoretical analysis confirming statement made in previous column.
2	Detune the second stage of HEMT.	Easy to do.	Follow-up temperature of 1.5 K will increase to 15 K if gain is reduced 10 dB.	Results of tests done on HEMT verify the statement in previous column. column.
3	Bypass HEMT and go directly from switch to downconverter.	None.	T_{op} increases. Difficult to implement changes in waveguide run.	—
4	Defocus subreflector.	Can easily lower 34-m antenna gain 12 dB to 17 dB by defocusing subreflector and not change zenith T_{op} very much.	Gain pattern affected. Main beam peak only about 6 dB above side lobe.	Might be good method for other applications but not for Sun experiments.
5	Place resistive sheets on top of horn aperture. (Suggested by R. Clauss.)	Easy to do. Resistive sheets of 188, 377, 277, 500 ohms per square are available in the lab.	Large mismatch interactions occur between sheet and horn. Can get only 6-db max gain loss using 188 ohm/square sheet.	Need to look into stacking 2 sheets to get more loss. Get theoretical predicts of gain loss and T_{op} increases.
6	Place polyurethane carbonized absorber sheet on top of horn aperture. Absorber can have desired 12-dB loss and symmetrical properties looking into either side of sheet.	Easy to do. T_{op} off source of 326 K and on Sun of 475 K can be achieved with 12-dB loss absorber sheet. T_{op} values close to calibrated linear region of	Need to fabricate absorber sheet with desired loss and VSWR characteristics. Need to calibrate loss of sheet for Ka-band system in which used.	Fabricated absorber sheet with 9-dB loss. Developed method for calibrating loss of absorber sheet as used in BWG system. Used this "absorber method" to obtain results reported in article.
7	Use the Ka-band system as is except reduce receiver system gain with a waveguide variable attenuator that should already be installed between output of HEMT and input to downconverter.	Easy to do if variable attenuator is already installed.	Even with added attenuation to reduce Sun signal going into receiver, difficult to verify that receiver is operating in linear region when antenna points at Sun. After tests, must restore original receiver configuration.	Used this "waveguide attenuator method" to obtain results in article.

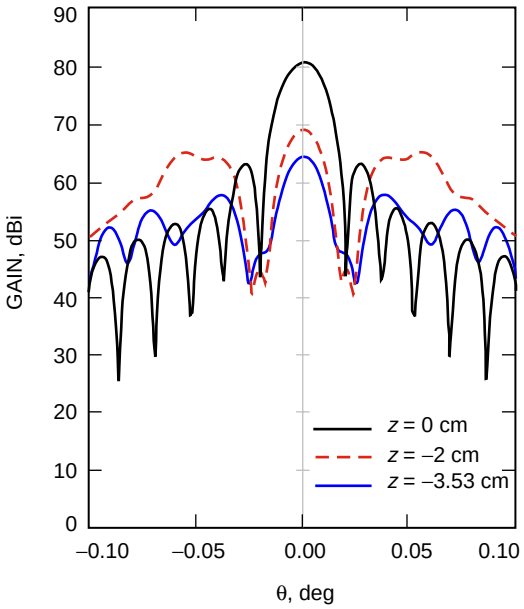

Fig. 1. 34-m BWG antenna gain patterns at 32 GHz for ϕ = 0- and 90-deg cuts and subreflector defocus positions z = 0, –2, and –3.53 cm.

34-m or 70-m antenna receiving system. The receiving system calibrations, which were done without the absorber sheet, do not have to be redone for the system configuration with the absorber sheet.

Determination of the absorber sheet loss was the most difficult aspect of the entire absorber method development. As will be shown later, the actual loss calibration is done when the absorber sheet is actually used in the antenna receiving system. Flat absorber sheets were special ordered from Advanced Electro Magnetics, Inc., located in Santec, California. The procurement specifications were that (1) the overall flat sheet be made of laminated carbon impregnated flat layers, (2) the total thickness should not be greater than 0.953 cm (0.375 in.), (3) the overall one-way transmission loss be about 13 dB when measured in free space for a normal incidence angle at 32 GHz, (4) the voltage standing wave ratio (VSWR) be less than 1.10 at its designated input side at 32 GHz, and (5) the top surface have a blue-colored coating for identification purposes.

These flat absorbers are manufactured by gluing together different layers of polyurethane foam material. Each layer is impregnated with a different density of carbon material. The input-side layer has the least amount of impregnated carbon while the output side has the most. The particular absorber sheet purchased from this manufacturer was made in three laminated layers. In an attempt to meet the VSWR requirements, the author modified the test piece as follows. First the procured absorber sheet was cut apart at the two-layer line with a razor blade. Then, from this two-layer piece, two identical round circles (slightly larger than the horn aperture) were cut. The final step was to glue the pieces back to back such that the designated input side (blue in color) was on both the front and back of the new test piece (see Fig. 2). By modifying the absorber in this manner, the modified absorber sheet was now symmetrical looking into either the input and output side. The input and output VSWRs were expected to be better than those of the original unsymmetrical sheet. Figure 2 shows a view of the edge and laminations of the absorber sheet. Figure 3 shows the absorber sheet and its aluminum ring holder. The holder was used only to ensure that the absorber test piece would lie on top of the horn aperture the same way each time it was used. Also since the absorber sheet tended to warp, the holder also ensured that the sheet would lie flat on the horn aperture.

Fig. 2. Close-up view of the outer edge of the absorber sheet cut to cover the horn aperture. Note the four laminated layers.

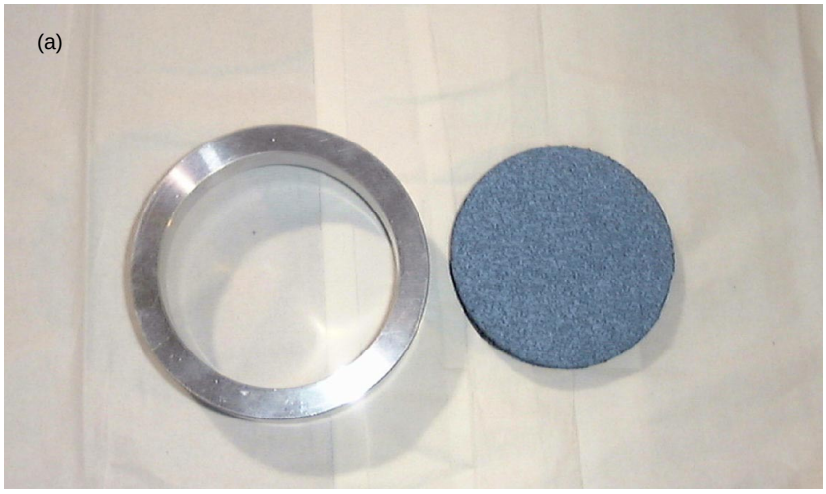

Fig. 3. Absorber sheet and holder: (a) absorber outside of the holder and (b) absorber sheet installed in the holder (as viewed from above the horn).

Several methods were tried for determining the loss of the absorber-sheet test sample that was manufactured. The first method involved measuring the horn gain and patterns without and with the absorber sheet at 32 GHz. The measurements were made on the near-field antenna range in the Microwave Engineering Laboratory located on the seventh floor of JPL Building 238. Figures 4 and 5, respectively, show measured E- and H-plane horn patterns without and with the absorber sheet (and sample holder) on the aperture of a laboratory Ka-band horn that was available. It can be seen from these figures that the horn patterns without and with the absorber are very similar in shape except for slight differences. The differences are that with the horn absorber and absorber holder (1) the beamwidth is slightly wider and (2) the side-lobe structures are slightly unsymmetrical. The horn gains for the two configurations (with and without absorber) were determined from pattern integrations of the E- and H-plane patterns. The gain of the horn with the absorber was lower than the gain without the absorber by 8.18 dB. This value is the absorber loss when the sheet is placed on the particular Ka-band horn used in these gain measurements. If different horns and receivers are used to measure the absorber-sheet loss, differences (1) in mismatch interactions between receiver, horn, and absorber sheet and (2) in the higher-order mode losses at the horn apertures will cause differences in the measured absorber-sheet losses.

At the author's request, Bob Thomas[2] of JPL did an independent study of absorber loss as a function of absorber test sample location at the horn aperture and also inside a Ku-band (17 GHz) circular waveguide feed horn. The Ku-band horn had an aperture diameter of about 14.2 cm (5.6 in.) and three

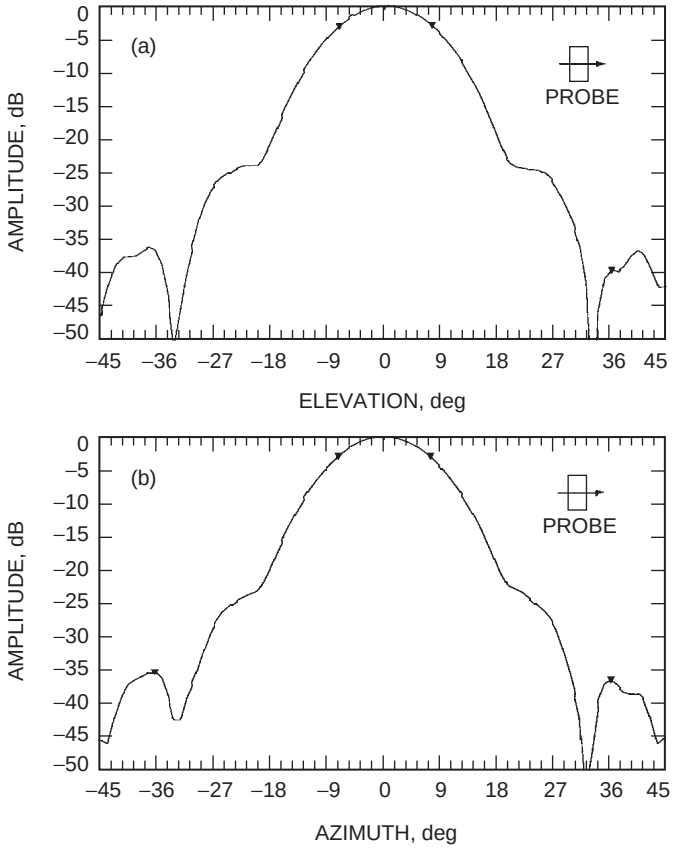

Fig. 4. The Ka-band horn (a) H-plane and (b) E-plane patterns at 32 GHz for no absorber sheet on the horn aperture. The probe is 3.81 cm from the horn aperture.

[2] B. Thomas, personal communication, Jet Propulsion Laboratory, Pasadena, California, February 9, 1998.

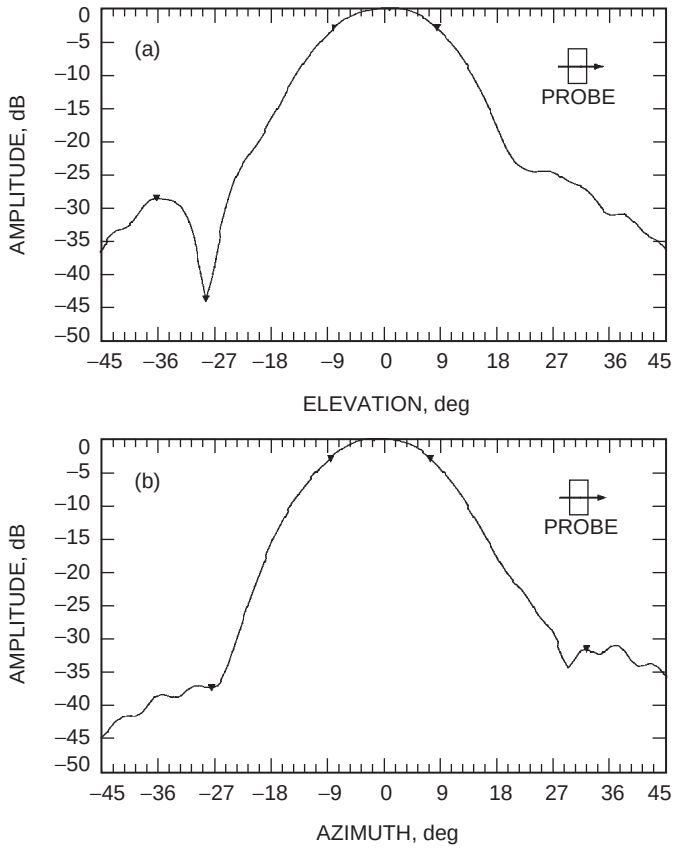

Fig. 5. The Ka-band horn (a) H-plane and (b) E-plane patterns at 32 GHz for absorber sheet and holder on the horn aperture. The probe is 3.81 cm from the horn aperture.

choke grooves on the horn aperture flange. The absorber test sample was made back-to-back similarly to the test sample made for Ka-band (see Fig. 2). The Ku-band sample had an absorber-sheet diameter that was 14.9 cm (5.85 in.) instead of the 8.9 cm (3.5 in.) for the Ka-band horn. Thomas systematically cut the absorber sheet to smaller and smaller diameters as he positioned the circular absorber sheet further and further down the horn. At each new absorber sheet location, measurements were made of the far-field gain of the horn with the absorber sheet. First a reference gain measurement was made with no absorber, and then the gain was measured with the absorber sheet on the horn aperture. The change in gain or gain loss was −18.4 dB, which was attributed to the loss of the absorber when placed on the horn aperture. The gain loss decreased progressively as the absorber was moved down the horn away from the horn aperture. The final gain loss was −13.7 dB when the absorber sheet was cut and located near the horn throat. This result shows that the loss is at maximum when the absorber sheet is placed on the horn aperture. The large −18.4 dB loss of the absorber sheet placed on the horn aperture was much higher than a −8.18 dB value obtained from similar tests done at 32 GHz.

The final laboratory method attempted for measuring the absorber-sheet loss was to make a rectangular block test sample cut to fit inside a WR28 guide. At 32 GHz, the VSWRs at the input and output sides of the WR28 absorber sample were measured to be 1.14 and 1.16, respectively, and the insertion loss was only 4.3 dB. The reason for this low loss value was attributed to the imperfect test sample cut to fit inside the WR28 guide. If the sample does not make good contact with the waveguide walls, leakage through the air gaps will cause the measured loss to be lower than the loss value for a perfectly cut sample. It is also known that WR28 supports propagation of a single TE_{10} mode at 32 GHz. A rectangular waveguide

measurement is equivalent to a free-space measurement of the absorber-sheet reflection and transmission properties for perpendicular polarization and an incidence angle equal to arcsin (f_c/f), where f is the test frequency of the test and f_c is the cutoff frequency of the WR28 waveguide. The loss of the absorber sheet in free space could be considerably lower than the multimode loss of the absorber sheet when it is placed on the horn aperture.

Loss determination based on zenith noise-temperature measurements was investigated next. It seems that the desired absorber loss could be determined by simply measuring zenith T_{op} values without and with the absorber sheet on the feed horn of the particular receive system with which the Sun experiments would be performed. However, derived equations for T_{op} (with and without the absorber sheet) showed that, in order to extract absorber-sheet loss based on zenith T_{op} measurements only, one needs to know the values of all the noise contributors, starting with the cosmic background radiation, the atmospheric loss noise, the main and subreflector losses (with spillover, cross polarization, and tripod contributions), and the BWG losses between f1 and f3. Focal point f1 is the focal point of the Cassegrain antenna at the reflector surface, and focal point f3 is the final focal point of the particular BWG receiving system horn installed inside the subterranean room. Even though these contributions were tabulated when the DSS-13 BWG antenna was first made and tested [5], changes in the mirror alignments and feed systems and main reflector backup structures have been made since that time. Since all of the individual noise contributions in a BWG system are not generally known, this method of determining absorber sheet loss was abandoned.

The method that would give the desired absorber loss values for any receive system was finally found. This final method consists of measuring the noise temperature of a radio source with and without the absorber sheet placed on the horn aperture of the receive system with which the Sun experiments were to be performed. The first radio source used was Venus. The measured Venus source temperature was found to be too small when the absorber sheet was placed over the horn. Loss calibrations were also attempted using Jupiter as a radio source, but, during these tests, Jupiter was only available at the end of Jupiter tracks when Jupiter was at 15-deg elevation angle or lower. At low elevation angles, errors were introduced due to tripod ground-noise pickup and increasing atmospheric loss effects at low elevation angles.

The Moon was found to be the best source to use for absorber-sheet loss calibrations because of its high source temperature and high elevation angles at 32 GHz (see Figs. 6 and 7). At the time of calibration on day of year (DOY) 325, the Moon was at Quarter Moon. The Quarter Moon was sufficiently illuminated to enable accurate source-temperature measurements with and without the absorber sheet. Figure 6 shows the system noise temperatures measured when scanning the Quarter Moon without and with the absorber sheet. The peak Moon temperatures without and with the absorber sheet were 188.10 K and 23.95 K, respectively. The ratio of the two peak temperatures gave a loss ratio of the absorber of 7.85, corresponding to a loss of 8.95 dB. This loss-ratio value for the absorber sheet was used for all of the absorber-method Sun measurements reported in this article. A similar measurement, made on DOY 347 (see Fig. 7) when the Moon was at Full Moon, resulted in the absorber sheet having a loss ratio of 8.08, corresponding to a loss of 9.07 dB. The Quarter Moon and Full Moon results agreed to within 2.9 percent. These results are significantly different from the 8.18-dB loss measured when the near-field antenna pattern range was used. Once the absorber sheet is determined for the Ka-band horn configuration, the absorber sheet calibration does not have to be repeated if new Sun measurements are done with the same receiving system on another day.

B. Waveguide Attenuator Method

The waveguide attenuator method involves the use of a WR28 variable attenuator that is installed between the output of the LNA and the input of the downconverter mixer of the Ka-band monopulse feed receiving system. This method assumes that, in the normal configuration, the high Sun noise temperatures will not saturate the LNA but will saturate the downconverter. The variable attenuator is

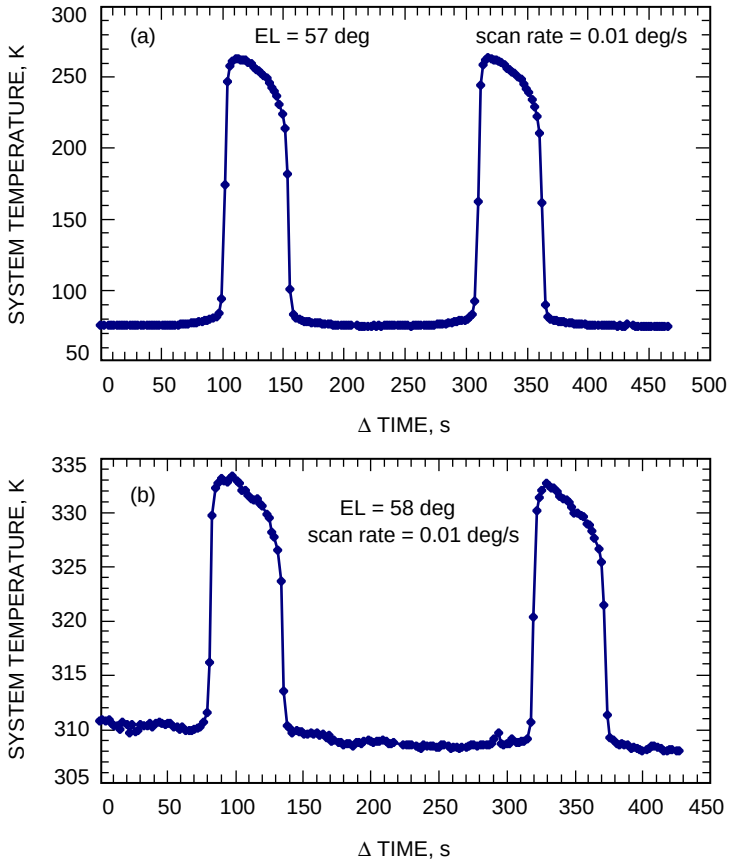

Fig. 6. Scans of the quarter moon (a) without and (b) with the absorber sheet, 32 GHz, 2000 DOY 325 (November 19). The leading edge of the scan was the lit side of the Moon. Note that the scan for (b) was started 1 minute after the end of the scan for (a). Delta system temperature is about 188 K in (a) and 24 K in (b).

used to attenuate the Sun's noise power such as to bring it into the linear region of the downconverter. Figure 8 shows a variable attenuator that is the same model of the one already installed. For the waveguide attenuator method, the setup procedure was to first point the antenna at the Sun. When this was done, the computer monitor for the noise-temperature calibration system displayed a system temperature value of infinity. The next step was then to gradually turn the attenuator screw adjustment on top of the attenuator (see Fig. 8) so as to increase the attenuation until the monitor showed system temperature values of about 6500 ± 100 K. Since the attenuator did not have a calibration dial mounted on it, it was not possible to know how much attenuation was added in. However, based on power meter readings, it is known that at least 5 dB of attenuation was added. This screw adjustment position was kept fixed for the rest of the measurements on the Sun. The final step was to measure the follow-up receiver temperature by the Y-factor on–off method described in [6]. For the Sun experiment results reported in this article, the follow-up noise-temperature contribution increased from 2.84 K to a surprisingly high value of 21.9 K.

The final step was to input this new measured follow-up noise temperature of 21.9 K into the system temperature calibration program, Topcal, developed by Stelzried [7] for DSS 13, and to perform full calibrations of the system. After the Sun noise-temperature measurements were completed, it was necessary to adjust the attenuator so that the attenuation was back to its original value so that the station was put back to its normal operating configuration. To verify that the attenuator was set back correctly, a new measurement of the follow-up temperature was required and checked against the original value. A

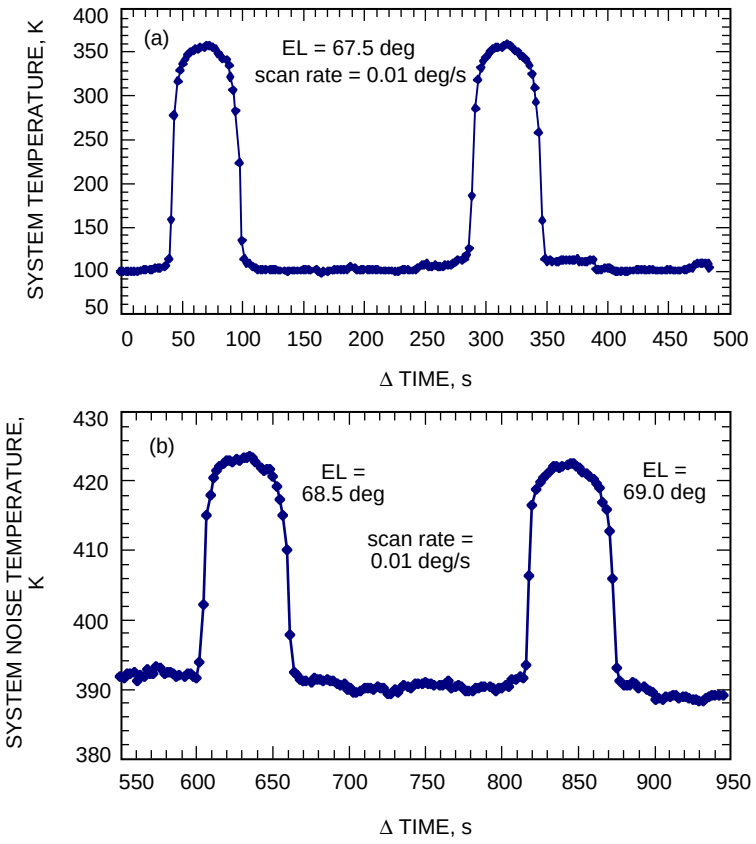

Fig. 7. Scans of the full moon (a) without and (b) with the absorber sheet, 32 GHz, 2000 DOY 347 (December 11).

Fig. 8. Type of WR28 variable attenuator used for the waveguide attenuator method.

significant disadvantage of this method is that this entire setup procedure has to be repeated if new Sun tests are done again with the same receiving system on another day.

III. Measurement Procedure and Data Reduction Method

The initial goal of the Sun Experiment Task was to find a way to measure the Sun noise temperature only at the Sun's center. The procedure was to start from different offsets from the Sun center and then move directly to the Sun's center for an on-source temperature measurement. The starting point offsets were ±5 deg in cross-elevation (XEL) and ±5 deg in elevation (EL). The measured Sun noise temperatures differed as much as ±20 K starting from the four different offsets. It was concluded that reliable Sun temperature data could not be obtained with this procedure. A decision was made to expand the objective of the Sun Experiment Task to measuring the Sun temperatures over the entire solar disk and not just at the center.

It is convenient to think of the Sun as a circle (disk) that has a radius of 0.25 deg and that the center of the Sun is the origin of an x–y coordinate system. The x- and y-axes are called the XEL and EL offset axes, respectively, and the offsets are measured from the Sun center in units of deg. The procedure developed for mapping the entire solar disk was to select a particular fixed EL offset and measure system temperatures while scanning the Sun in XEL offsets from −1.2 deg to +1.2 deg. After this scan, another XEL offset scan was made for a new EL offset. This scanning procedure was continued until the entire solar disk plus close-in regions were mapped for −0.35 deg to 0.35 deg EL offsets in increments of 0.05 deg. The XEL scan rate was 2.666 mdeg/s, and data were taken every 2 seconds. Measured system temperature values were permanently recorded in a computer data file. In the post-processing, the noise temperatures recorded in time are converted to noise temperature-versus-XEL offset and plotted. Any portions of the measured noise-temperature curves can be expanded to see detail to a resolution of 5.332 mdeg in XEL. These expanded plots might be useful to telecommunications engineers who are interested in knowing what the system temperature increases are in the close-in regions of the Sun [4].

After measuring the system temperature by the described experimental procedure, the data-reduction procedure involved subtracting out the minimum system temperature measured when the antenna was in the region of −1.2 deg to −0.6 deg XEL from the system temperatures measured at the other XEL angles. The next step was to correct the above differenced data for the absorber-sheet loss. The final steps were to correct for the atmosphere loss and the antenna system efficiency. These data reduction steps are expressed mathematically as

$$T_{\text{sun}} = \frac{[(T_{op})\text{on} - (T_{op})\text{off}] \times L_{abs} \times L_{atm}}{\eta} \times C_r \tag{1}$$

where (T_{op})on and (T_{op})off are the system temperatures measured when the antenna points at the Sun and off the Sun, respectively; L_{abs} is the power loss ratio of the absorber sheet; and $Latm$ and η are, respectively, the atmosphere loss factor and the antenna efficiency at the elevation angle at which the Sun measurements were made. For the waveguide attenuator method, $L_{abs} = 1$, and for the absorber method, $L_{abs} = 7.85$ (see the discussion in Section II). The symbol C_r is the source size correction factor. If the nonlinearity factor of the receiving system is known accurately, Eq. (1) is multiplied by the nonlinearity factor.

Equation (1) was derived from mathematical manipulation of the antenna efficiency formula given in [8] as

$$\eta = \frac{\Delta T \times L_{atm}}{\left[\dfrac{T100}{C_r}\right]} \tag{2}$$

where

$$\Delta T = (T_{op})\text{on source} - (T_{op})\text{off source} \tag{3}$$

The delta term in Eq. (3) is sometimes referred to as the "system temperature increase" due to the radio source. The symbol T100 is the system temperature increase that would be measured for ΔT if the antenna system were perfect (i.e., 100 percent aperture efficiency and no losses in the antenna system between the aperture and the T_{op} measurement reference point). For the results presented in this article, T100 in Eq. (2) is T_{sun} in Eq. (1). A value of $C_r = 1$ was assumed for the results of this article because it is not presently known what the C_r value is for measurements on a source as large as 0.5-deg diameter with an antenna beamwidth of 17 mdeg. Performing a theoretical study to determine the correct C_r value is beyond the scope of this article. Some calculated antenna noise temperatures as measured when scanning the Sun with the 34-m antenna are given in the Appendix. When a value of C_r becomes known, the Sun temperatures presented in this article can be multiplied by the value of C_r [see Eq. (1)].

Rebold et al. [3] give a methodology for calculating the expected increase in system noise temperature of the Sun when observed by a 34-m high-efficiency antenna at 8.42 GHz. Their methodology will be studied for possible application to the calculation of expected Sun noise temperatures observed by a 34-m BWG antenna at 32 GHz.

For a BWG antenna system, the term antenna efficiency (or efficiency) is used to mean antenna efficiency that includes all losses of the Cassegrain antenna plus the losses between f1 and the receiver calibration reference point. For DSN systems, the calibration reference point is usually the input of the LNA [5]. For the DSS-13 BWG antenna with the Ka-band monopulse feed, the efficiencies were calculated from the following equations:[3]

For source rising,

$$\eta = 0.1807 + 0.0136019 \times \text{EL} - 0.000150694 \times \text{EL}^2 \tag{4}$$

For source setting,

$$\eta = 0.2415 + 0.015646 \times \text{EL} - 0.00019589 \times \text{EL}^2 \tag{5}$$

where EL is the elevation angle in degrees.

Table 2 shows the elevation angles and efficiencies corresponding to different EL offsets on the different test dates. Note that the elevation angles as functions of EL offsets were different for each of the test dates. The Sun was not scanned at close to the same elevation angles on the different dates because, on two occasions, the DSS antenna controller computer froze at the intended start of the test time. It took 2 to 3 hours to diagnose and correct the problems. As may be seen in Table 2, the Sun was already setting when the tests began on DOY 293.

The atmospheric loss factor, L_{atm}, at 32 GHz as a function of elevation angle for test dates DOY 244 and DOY 258 was determined from ground weather data using an Excel program furnished by S. Slobin of the Communications Systems and Research Section. For test date DOY 293, zenith atmosphere noise temperatures, measured at 31.4 GHz by the advanced water vapor radiometer (AWVR), were furnished by A. Tanner and S. Keihm of the Microwave and Lidar Technology Section. These measured zenith temperatures were converted to L_{atm}(EL) at 32 GHz using formulas furnished by S. Keihm.

[3] D. Morabito, personal communication, Jet Propulsion Laboratory, Pasadena, California, August 31, 2000.

Table 2. Elevation angle and efficiencies corresponding to EL offsets.

All test days		DOY 244 (August 31, 2000)			DOY 258 (September 14, 2000)			DOY 293 (October 19, 2000)			
See Fig.	EL offset, deg	EL angle, deg	Source rising or setting	Efficiency	EL angle, deg	Source rising or setting	Efficiency	EL angle, deg	Source rising or setting	Efficiency	Comments on 293 rising or setting
11	0.00	50.4	Rising	0.4835	57.6	Rising	0.4642	39.2	Setting	0.5538	Cont'd. from
12	0.05	52.9	Rising	0.4785	57.8	Rising	0.4634	38.2	Setting	0.5533	bottom of
13	0.10	55.4	Rising	0.4717	57.6	Setting	0.4928	37.1	Setting	0.5524	column
14	0.15	57.3	Rising	0.4653	57.1	Setting	0.4962	36.0	Setting	0.5508	
15	0.20	59.5	Rising	0.4565	56.4	Setting	0.5008	34.7	Setting	0.5486	
16	0.25	61.0	Rising	0.4997	55.3	Setting	0.5077	33.4	Setting	0.5455	
17	0.30	62.3	Rising	0.4432	53.3	Setting	0.5189	32.0	Setting	0.5415	
18	0.35	63.1	Rising	0.4390	52.0	Setting	0.5254	30.5	Setting	0.5365	
19	0.00	63.0	Setting	0.4497	45.8	Setting	0.5472	44.2	Setting	0.5503	Test started here
20	−0.05	62.6	Setting	0.4533	—	—	—	44.0	Setting	0.5506	
21	−0.10	61.5	Setting	0.4628	—	—	—	43.8	Setting	0.5511	
22	−0.15	60.7	Setting	0.4695	—	—	—	43.5	Setting	0.5515	
23	−0.20	59.0	Setting	0.4827	—	—	—	43.0	Setting	0.5521	
24	−0.25	56.8	Setting	0.4982	—	—	—	42.0	Setting	0.5531	
25	−0.30	55.1	Setting	0.5089	—	—	—	41.1	Setting	0.5537	
26	−0.35	52.7	Setting	0.5220	—	—	—	40.3	Setting	0.5539	Cont. at top of column

IV. Experimental Results

As confirmation that the absorber method would give valid results at different elevation angles, tipping curves were obtained with and without the absorber sheet. Figure 9 shows the tipping curves that were measured at 32 GHz for the Ka-band monopulse feed receiving system. The tipping curve measured for the absorber loss case was corrected for absorber loss and adjusted at the zenith value so that it could be superimposed on the tipping curve measured without the absorber. It can be seen that the two curves are very similar in shape. The deviations of the two curves are attributed to larger standard deviations that occurred when measuring system temperatures with the absorber on the horn. The reasonably good agreement in tipping curves verifies that slight antenna pattern distortions (see Figs. 4 and 5) for the absorber method will not cause large errors in Sun measurements as functions of antenna elevation angles.

The receiving system linearity is determined by measuring the amplitudes of the injected noise-diode temperatures when the LNA is connected first to the antenna and then to the ambient load thermal noise standard. The degree to which the injected noise-diode pulse magnitudes are the same in these two configurations is a measure of the receiver nonlinearity. Measuring the linearity or nonlinearity is part of the calibration sequence called mini-cal [7].

When the absorber sheet and holder were used on the DSS-13 Ka-band monopulse system, the system temperatures on and off the Sun were, respectively, about 1400 K and 308 K. Even though 1400 K is outside the calibrated linearity range of about 350 K, mini-cals performed with the antenna pointed at

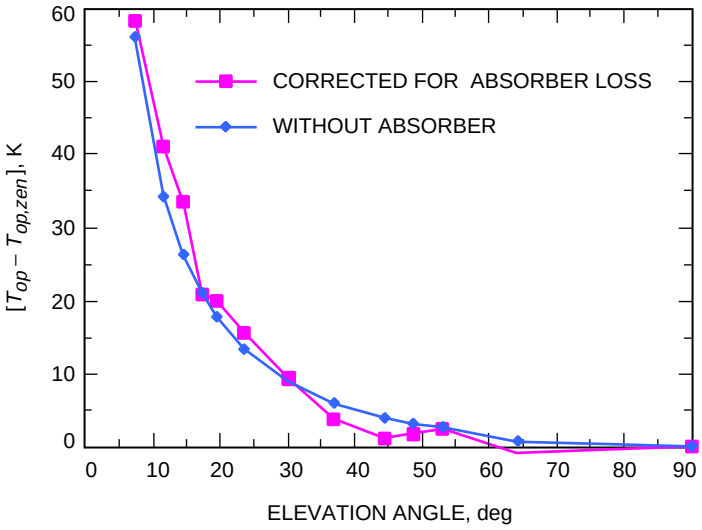

Fig. 9. Tipping curves of the 34-m BWG antenna at 32 GHz with and without the absorber sheet.

the Sun showed that the worst-case linearity factor was about 1.03 to 1.05. This nonlinearity corresponds to about a 3 to 5 percent error in measuring the Sun noise temperature. The causes of variation in measured linearity for the absorber method can be explained as follows. When the antenna was pointed at the Sun and the system temperature was about 1400 K, the standard deviations of the measured Sun temperature values every 2 seconds were about 2 K maximum. Standard deviations of this magnitude were significant, but were not large enough to mask out the injected noise-diode temperatures of about 16 K. For this method, one needs to do several mini-cals (or more) so that the linearity factors, measured while looking at the Sun, can be averaged. The averaging tends to smooth out the fluctuation effects.

Mini-cals that were performed while on the Sun for the waveguide attenuator method gave linearity factors that ranged from 1.01 to 2.0. The high linearity values are partly due to the fact that the noise-diode pulse magnitude is only 16 K, and the standard deviations of the measured Sun temperatures, while looking at the active Sun of about 6500 K, were varying from 3 to 21 K. The high standard deviations tend to mask out the injected noise-diode temperature pulses of about 16 K and cause errors in determining linearity. Therefore, it was not certain whether the measurements for the waveguide attenuator method were made in the linear region.

During the process of performing the Sun experiment measurements, it was puzzling to find that Sun temperature measurement results obtained with the absorber and waveguide attenuator methods disagreed by such large amounts. It was equally puzzling and discouraging to find that measurements made at the same EL offsets did not repeat. It was discovered later that Sun experiments reported in this article were being performed during a year of maximum solar activity. Figure 10 shows a plot of the Sun sunspot number versus year. The sunspot number is a measure of solar activity. Note that the solar sunspot cycle is approximately 11 years and that year 2000 was a year of maximum solar activity. Due to the high solar activity during the experiments, it was not even possible to repeat measurements on different days or even on the same day. Solar flares (noise bursts) occurred on some of the Sun scans. The measurements with the absorber method were performed on DOY 244, which had a sunspot number of 157. This was much higher solar activity than for DOYs 257 and 298, when the measurements were made with the waveguide attenuator method. Solar activities on DOY 257 had a sunspot number of 60, and on DOY 293 the sunspot number was 90.[4] Figures 11 through 18 are measured Sun noise-temperature

[4] These sunspot numbers were found for year 2000 by going to the Internet address http://sidc.oma.be/DATA/DAILYSSN/dailyssn.html and then clicking on 2000 to get daily sunspot numbers for the year 2000.

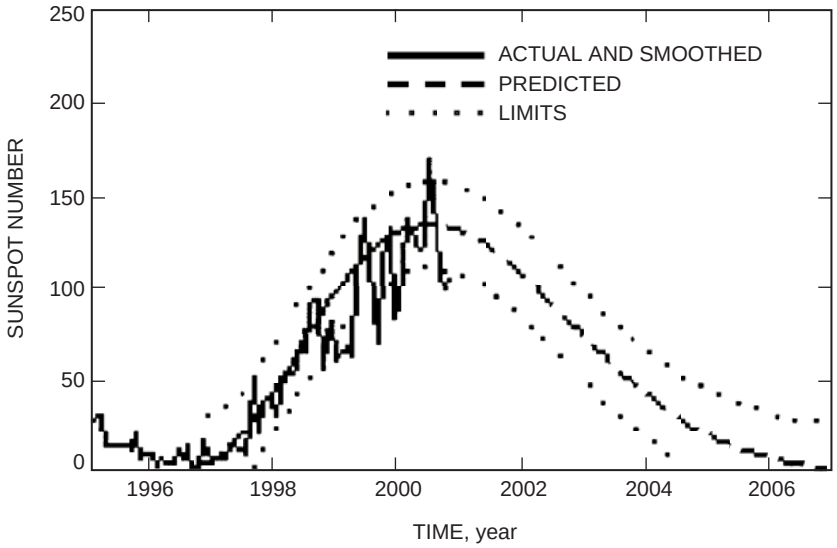

Fig. 10. Solar cycle from 1995 through 2007, showing that maximum solar activity occurred during the latter part of 2000. (This figure was obtained from http://wwwssl.msfc.nasa.gov/ssl/pad/solar/sunspots.htm)

plots for the upper half of the solar disk, while Figs. 19 through 26 are plots for the lower half of the solar disk. The range of EL offset values covered was from −0.35 to 0.35 deg in 0.05-deg increments. All plots show the features near the edges of the solar disk.

To facilitate comparisons and to reduce the number of plots presented in this article, the results for 2000 DOY 244, 258, and 293 are superimposed. For DOY 258 measurements, there was only enough time to complete measurements of the upper half of the solar disk. On DOY 293, to ensure that both halves of the solar disk were measured, the XEL scans were abbreviated to −0.6 deg to 0.6 deg.

As was shown in Eq. (1), three correction factors must be applied to the measured system temperature increase in order to arrive at the value of $T_{\rm sun}$. These correction factors, applied in sequence, are L_{abs}, L_{atm}, and the antenna efficiency. In Figs. 11 through 26, it is of interest to show the results before and after the efficiency corrections were made. Showing both sets of curves often yields information that is not revealed from examining only the final $T_{\rm sun}$ values (obtained after the efficiency corrections were made). However, in order to keep this article from becoming too long, only Figs. 11 and 19 will be presented with curves uncorrected and corrected for efficiency. All other results in the Fig. 11 through Fig. 26 sequence will show only the $T_{\rm sun}$ values after making corrections for efficiency.

Figures 11 and 19 were selected for discussion purposes because they are the only figures that show the results of measurements repeated at the same EL offset angle. Even though the EL offset angle of 0.0 deg is the same for Figs. 11 and 19, the measurements were made at different elevation angles and, therefore, different efficiency corrections had to be applied. To facilitate this discussion, the elevation angle and efficiency information from Table 2 was incorporated into Figs. 11(b) and 19(b).

Note in Fig. 11(a) that the curves for DOY 258 and DOY 293 are close together, but after application of the efficiency corrections as shown in Fig. 11(b), the two curves are separated by a significant amount. In Fig. 11(a), the efficiency corrections to be applied to these closely spaced curves are shown to be 0.464 and 0.554 for DOY 258 and DOY 293, respectively. This large separation of the two curves in Fig. 11(b) is therefore due to the significant difference in the efficiency corrections. Now make similar observations of the curves in Fig. 19. Note that in Fig. 19(a) the curves for DOY 258 and DOY 293 are again close together. The efficiency corrections to be applied are shown in Fig. 19(b) to be 0.547 and 0.550, respectively. These two corrections are nearly the same in values and, therefore, after application

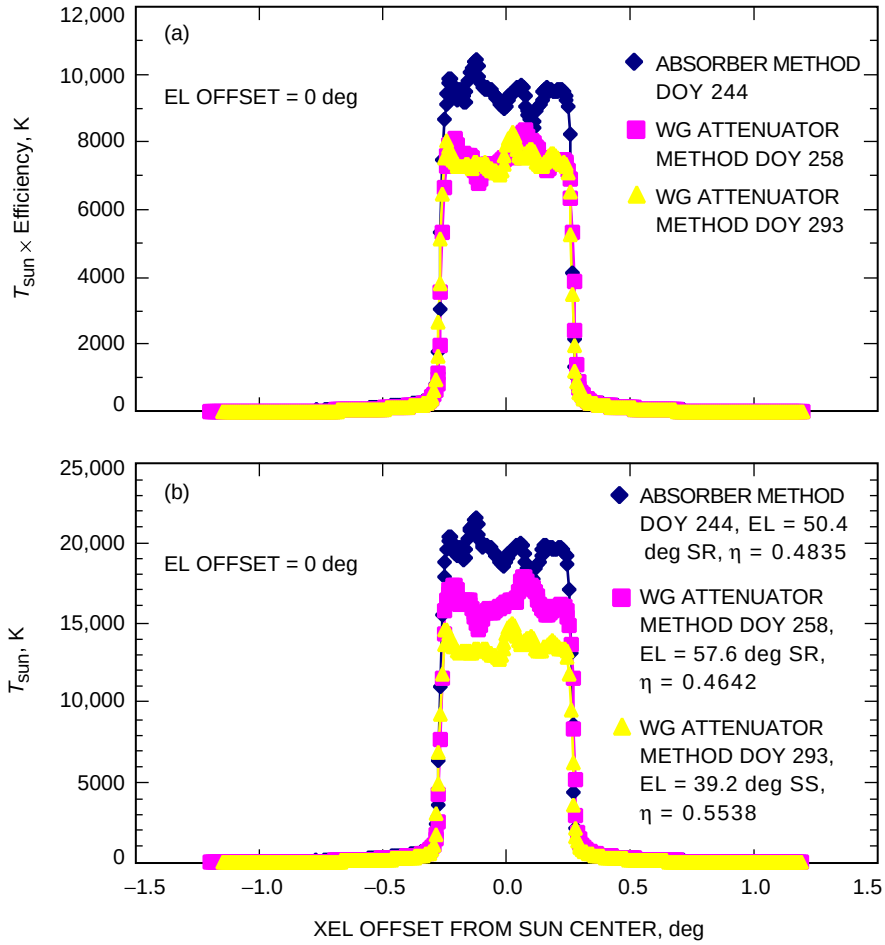

Fig. 11. DSS-13 BWG antenna, XEL Sun temperature profile for EL offset = 0.0 deg, 32 GHz: (a) no corrections made for efficiency and (b) corrections made for efficiency. Efficiency values are functions of elevation angle and Sun rising (SR) or Sun setting (SS).

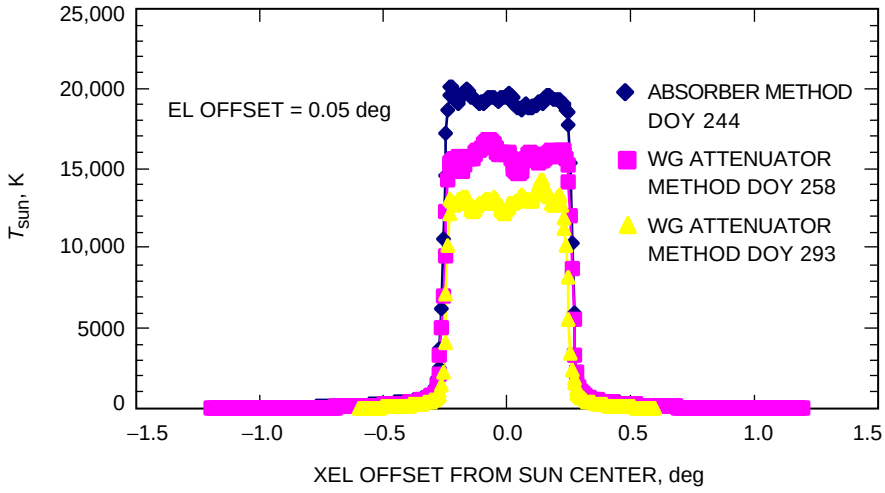

Fig. 12. DSS-13 BWG antenna, XEL Sun temperature profile for EL offset = 0.05 deg and 32 GHz.

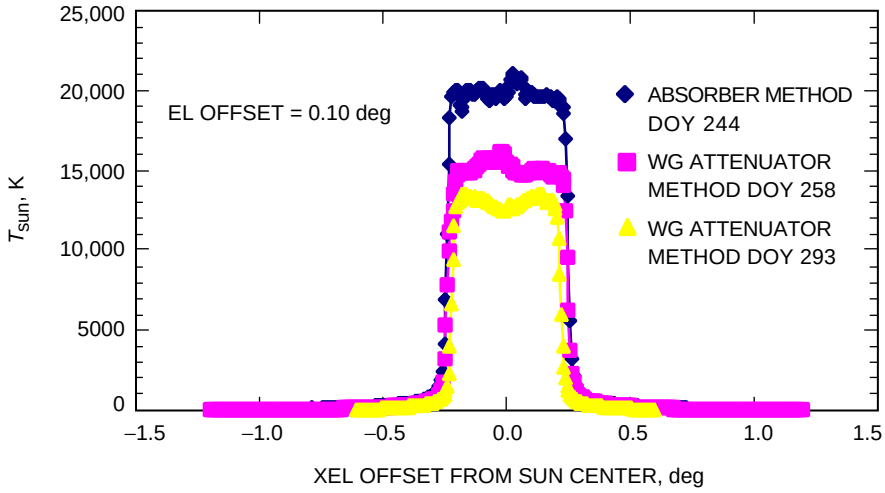

Fig. 13. DSS-13 BWG antenna, XEL Sun temperature profile for EL offset = 0.10 deg and 32 GHz.

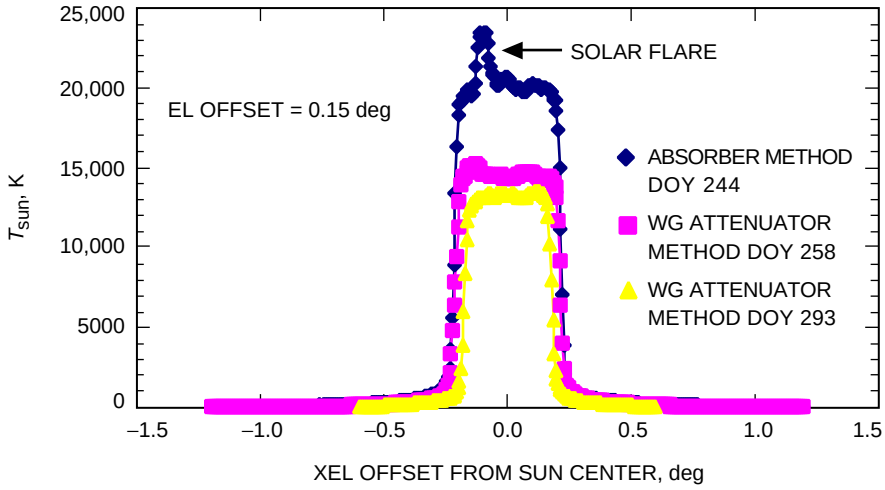

Fig. 14. DSS-13 BWG antenna, XEL Sun temperature profile for EL offset = 0.15 deg and 32 GHz.

to the DOY 258 and DOY 293 curves in Fig. 19(a), the curves in Fig. 19(b) remained close together. Without knowledge of the efficiency correction information, it would have been difficult to deduce the reason for the different separations of the curves for DOY 258 and DOY 293 in Figs. 11(b) and 19(b) after efficiency corrections were made.

It is of now of interest to compare the final $T_{\rm sun}$ values for all the test days shown in Figs. 11(b) and 19(b). The $T_{\rm sun}$ values for DOY 244 in Figs. 11(b) and 19(b) are 19,500 K and 20,500 K, respectively. The corresponding disagreement is 5.1 percent, which is acceptable considering that the efficiency corrections have some tolerances associated with them. The $T_{\rm sun}$ values for DOY 293 in Figs. 11(b) and 19(b) are each about 13,500 K, and are in very close agreement. The $T_{\rm sun}$ values for DOY 258 in Figs. 11(b) and 19(b) are about 16,000 K and 13,500 K, respectively, and the corresponding disagreement is 15.6 percent. The large disagreement for the $T_{\rm sun}$ values on DOY 258 might be due to non-repeatability of some measurements during a period of high solar activity. It is also possible that, since some changes occurred in the BWG system since 1998, the efficiency values at some elevation angles might also have changed. The efficiency equations [Eqs. (4) and (5)] might need to be updated. Also, there might be

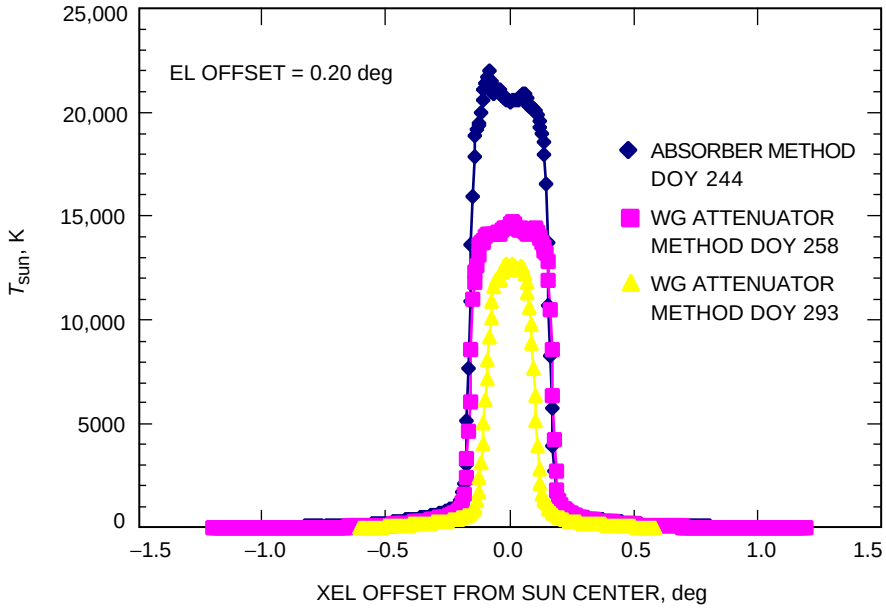

Fig. 15. DSS-13 BWG antenna, XEL Sun temperature profile for EL offset = 0.20 deg and 32 GHz.

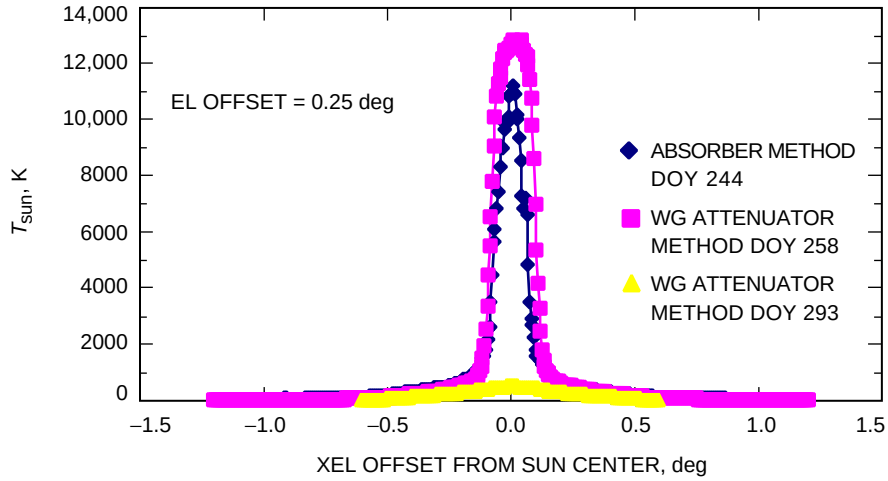

Fig. 16. DSS-13 BWG antenna, XEL Sun temperature profile for EL offset = 0.25 deg and 32 GHz.

some small residual errors in the efficiency corrections due to neglecting the effects of azimuth. However, to date, no published data are available for efficiency as a function of both elevation and azimuth angles.

Figure 27 shows the results of two scans for 0-deg EL offset, but taken one hour apart on the same day. It can be seen from the plot that the measurements on the Sun at the same EL offset were non-repeatable. Note that, for the scan taken one hour later, a solar flare occurred that was not there on the earlier scan.

Figure 28 shows Sun temperatures measured with the waveguide method for an EL scan made through the Sun center rather as an XEL scan. It is the only EL scan that was done and was the final measurement that was made for the Sun experiment. It is of interest to compare the temperature profile measured for the EL scan through the Sun center in Fig. 28 with the profile measured for the XEL scan through the Sun center in Fig. 11.

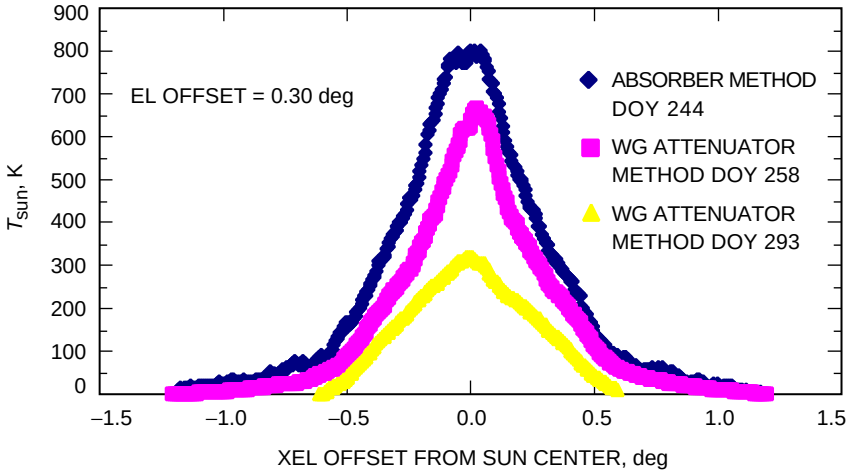

Fig. 17. DSS-13 BWG antenna, XEL Sun temperature profile for EL offset = 0.30 deg and 32 GHz.

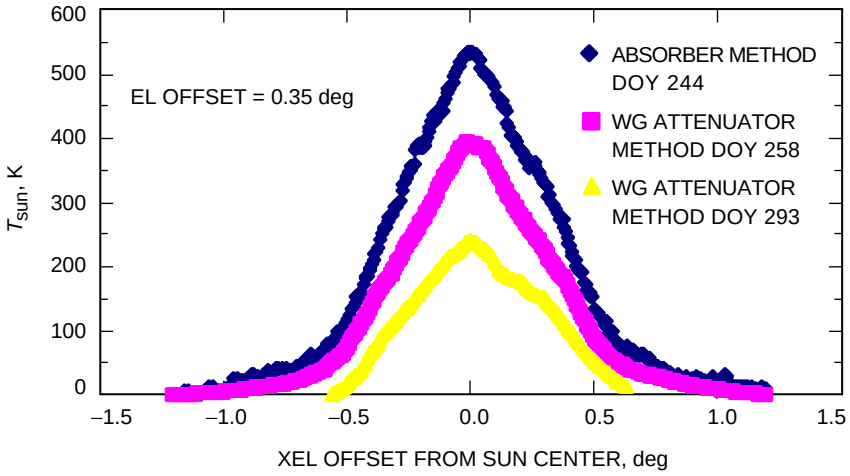

Fig. 18. DSS-13 BWG antenna, XEL Sun temperature profile for EL offset = 0.35 deg and 32 GHz.

Figures 11 through 15 and 19 through 24 show that the noise temperatures over the Sun surface varied considerably. For example, the Sun temperature in Fig. 11(a) for DOY 244 has (1) a mean value of about 9425 K across the Sun surface, (2) a peak value as high as 10404 K, and (3) a minimum value as low as 8420 K. These peaks and values represent deviations from the mean of +979 K and −1005 K. Figures 14, 19, 20, 23, and 28 show that solar flares had occurred during the scans. Figures 16 through 18 and Figs. 24 through 26 show residual Sun noise temperatures for |EL offsets| => than the Sun's radius. The reason the Sun noise temperatures are not zero at these EL offsets is because portions of the antenna beam still lie inside the Sun's perimeter. Figure 24 shows high Sun temperatures at −0.25 deg (or at the Sun's edge for the lower half of the disk) because the Sun's center in the EL direction was not known accurately or perhaps because the Sun is not radiometrically a perfect circular disk.

The exact location of the Sun center was not known a priori even though in all of the figures it appears that the XEL scans are centered about the Sun center. The reason the curves appear centered is because, in the post-processing, the data were shifted in XEL the appropriate number of degrees (0.024 deg max) necessary to make the scanned Sun curves be centered about the Sun center.

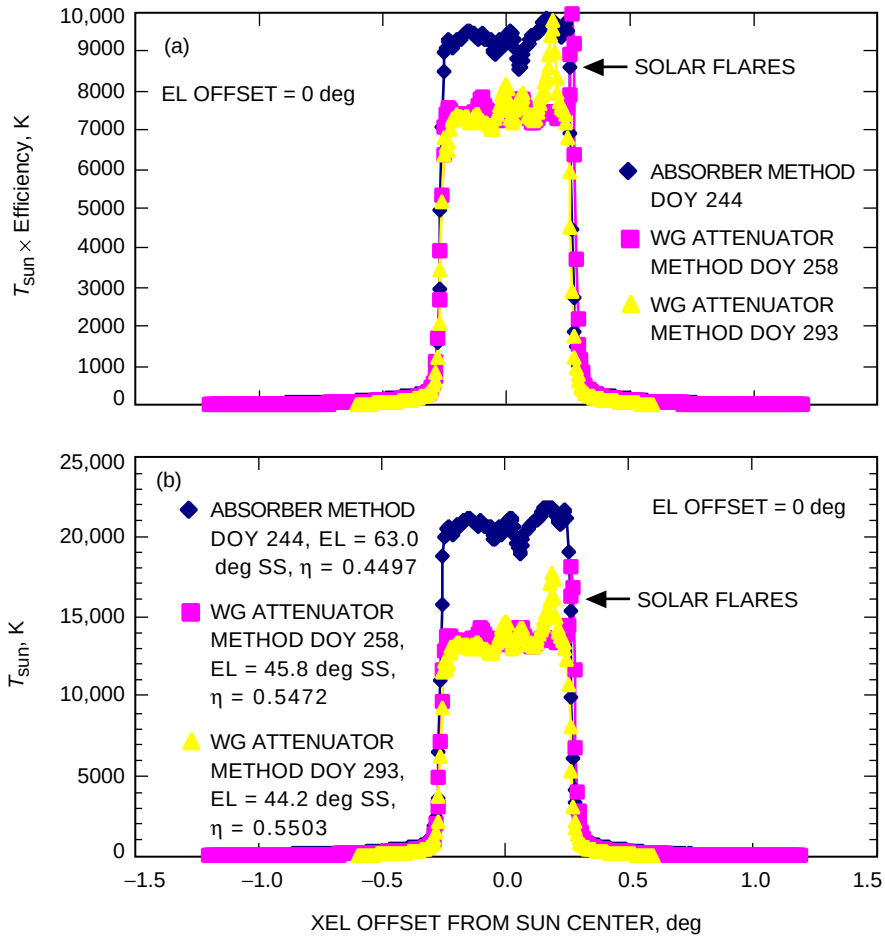

Fig. 19. DSS-13 BWG antenna, XEL Sun temperature profile for EL offset = 0.0 deg (repeat), 32 GHz, atmosphere loss removed: (a) no corrections made for efficiency and (b) corrections made for efficiency. Efficiency values are functions of elevation angle and Sun rising (SR) or Sun setting (SS).

Even though the Sun center for the XEL scan could be determined from scanning continuously across the Sun surface in XEL, the location of the Sun center in the EL direction was not known as accurately. Except for the final scan shown in Fig. 28, no scans were taken in the EL direction. Initially, boresight methods were used to try to find the center, but they proved to be inadequate. Therefore, the EL offsets from the true Sun horizontal centerline were probably in error. If the offsets in EL are referenced to the true Sun's horizontal centerline, the full beamwidth of the Sun as determined from the XEL scans should be

$$W = 2 \times \sqrt{R^2 - H^2} \tag{6}$$

where W is the full Sun beamwidth in deg, R is the radius of the Sun in degrees (assumed to be 0.25 deg), and H is the elevation offset in degrees. When EL offset H is zero, W becomes 0.5 deg. At the edge of the solar disk, H is 0.25 deg and Wwill be 0. If the Sun's center is not correctly located, the measured full beamwidth of the Sun will deviate from the above relationship by a significant amount when H approaches R. For example, if the error in finding the true Sun's center is ± 0.02 deg in EL, the measured total width of the Sun in degrees will be

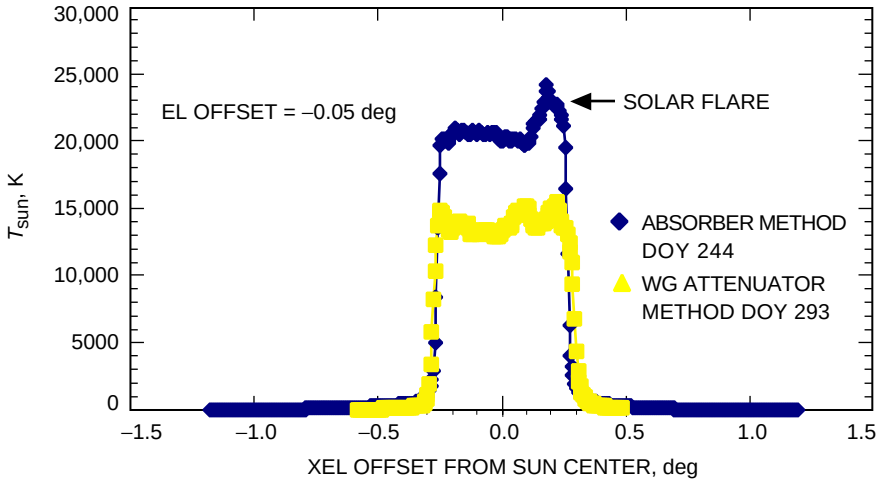

Fig. 20. DSS-13 BWG antenna, XEL Sun temperature profile for EL offset = –0.05 deg and 32 GHz.

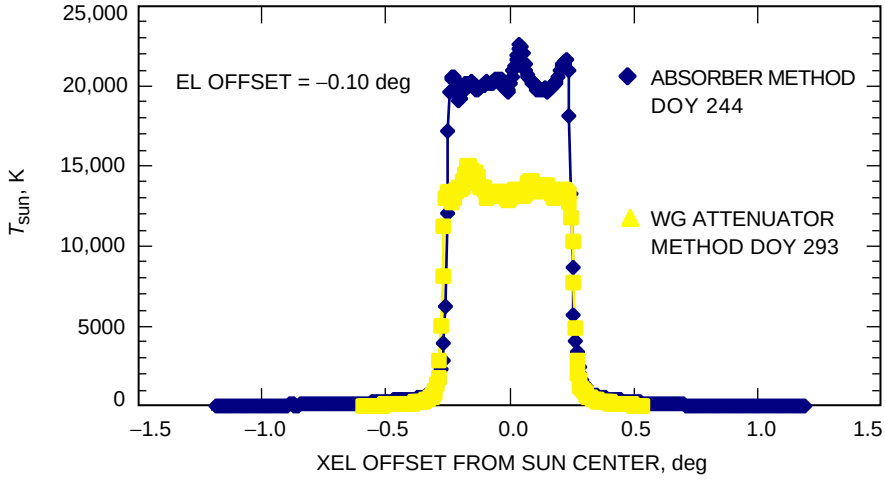

Fig. 21. DSS-13 BWG antenna, XEL Sun temperature profile for EL offset = –0.10 deg and 32 GHz.

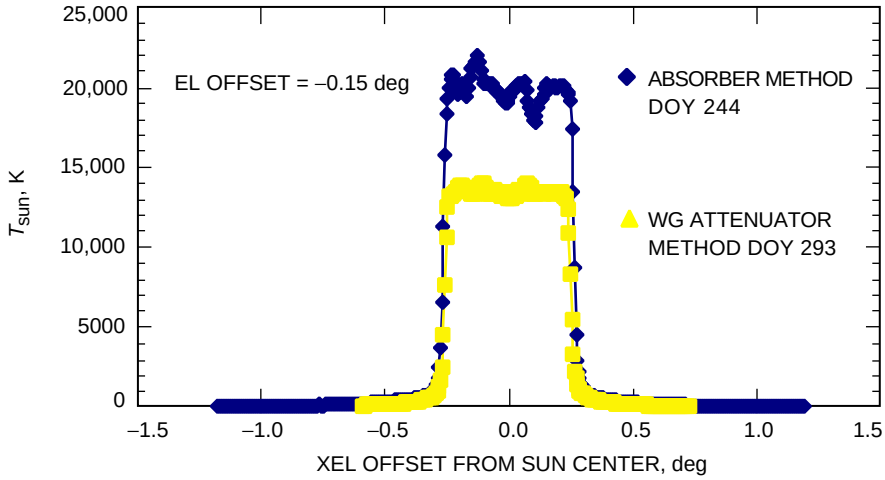

Fig. 22. DSS-13 BWG antenna, XEL Sun temperature profile for EL offset = –0.15 deg and 32 GHz.

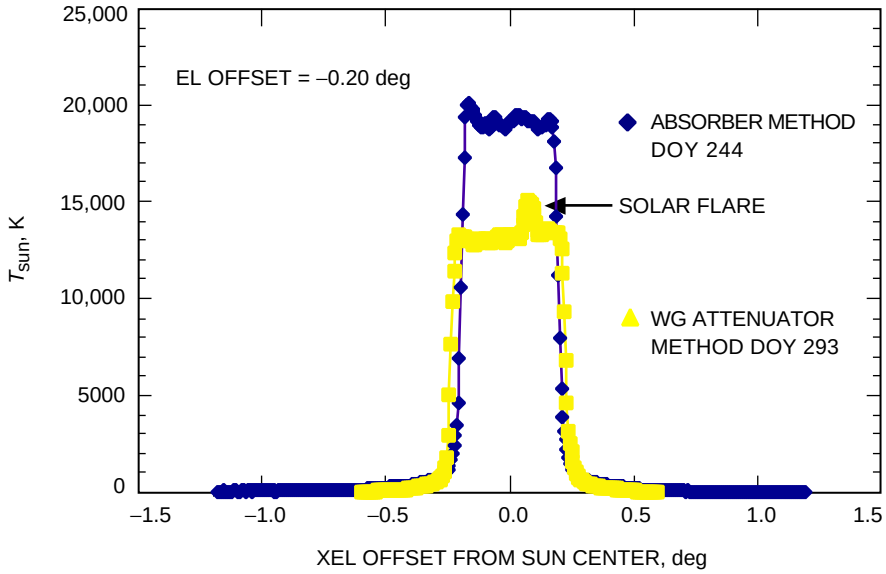

Fig. 23. DSS-13 BWG antenna, XEL Sun temperature profile for EL offset = –0.20 deg and 32 GHz.

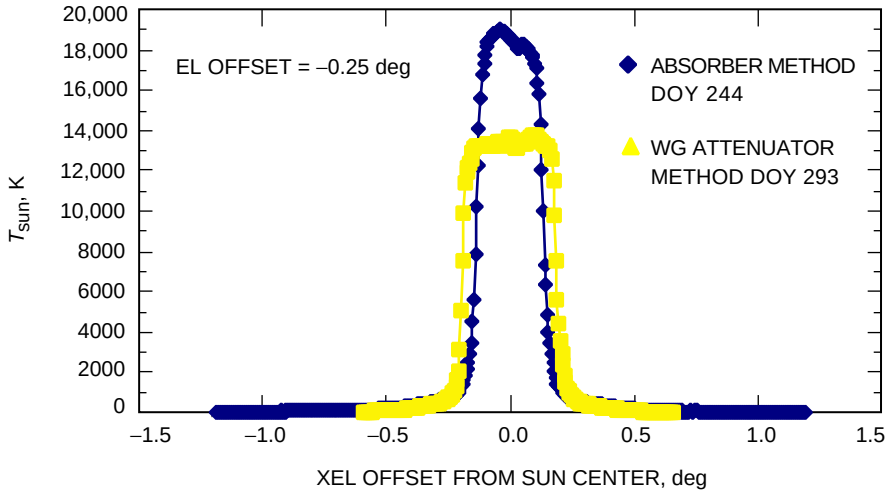

Fig. 24. DSS-13 BWG antenna, XEL Sun temperature profile for EL offset = –0.25 deg and 32 GHz.

$$W' = 2 \times \sqrt{R^2 - (H \pm 0.02)^2} \tag{7}$$

for positive values under the radical sign.

The error in W is just

$$\Delta W = W - W' \tag{8}$$

The changes of W are barely noticeable for small values of H, as can be seen in the experimental results. However, as the values of H approach ± 0.2 deg, the changes in W as a function of H become very

noticeable. For example, if the value of H is exactly 0.2 deg and R is 0.25 deg, from Eq. (6) W is calculated to be 0.30 deg. However, if H is in error by +0.02 deg on one test day and −0.02 deg on another day, then W' calculated from Eq. (7) would be 0.237 deg on one day and 0.347 deg on the other day instead of 0.3 deg. Note that, for the plots in Fig. 15 for the assumed value of 0.2 deg for H, the width of the DOY 293 T_{sun} curve is narrower than the curves for DOYs 244 and 258. This indicates that on one of the days or on all 3 days the experimental value assumed for H was not correct because the actual Sun center in EL was not known.

Examination of the figures shows that, for the same EL offsets, the results for the absorber method on DOY 244 were much higher that the results for the waveguide attenuator method (DOY 257 and DOY 293). These differences are attributed to the higher solar activity for DOY 244 (sunspot number = 157) compared to the moderate solar activities on DOY 257 (sunspot number = 60) and on DOY 293 (sunspot number = 90). Year 2000 happened to be a year of maximum solar activity (see Fig. 10). R. Woo states that the Sun temperature could be twice as hot during solar maximum as compared with the temperature during solar minimum. He also states that, during the year of a quiet Sun, the sunspot

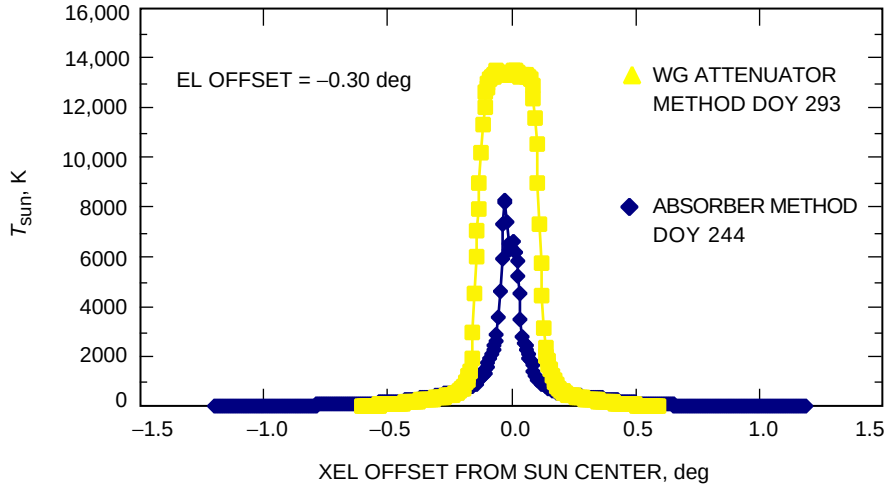

Fig. 25. DSS-13 BWG antenna, XEL Sun temperature profile for EL offset = –0.30 deg and 32 GHz.

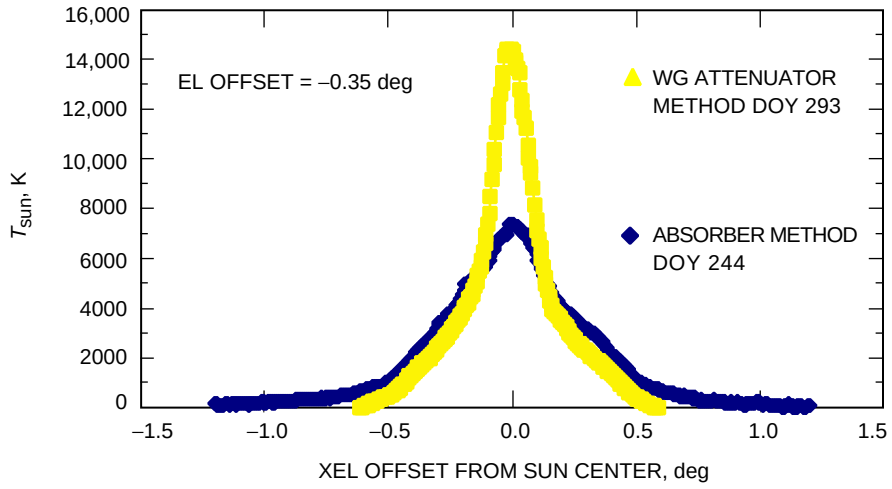

Fig. 26. DSS-13 BWG antenna, XEL Sun temperature profile for EL offset = –0.35 deg and 32 GHz.

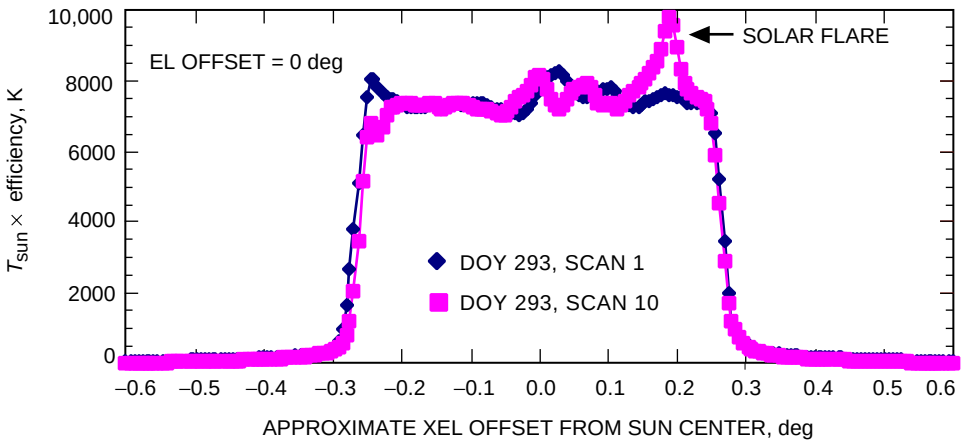

Fig. 27. Two XEL Sun scans superimposed to show non-repeatability. Scan 1 [Fig. 11(a)] and scan 10 [Fig. 19(a)] for the waveguide method and EL offset = 0 deg were done 47 minutes apart on the same day. No corrections made for efficiency.

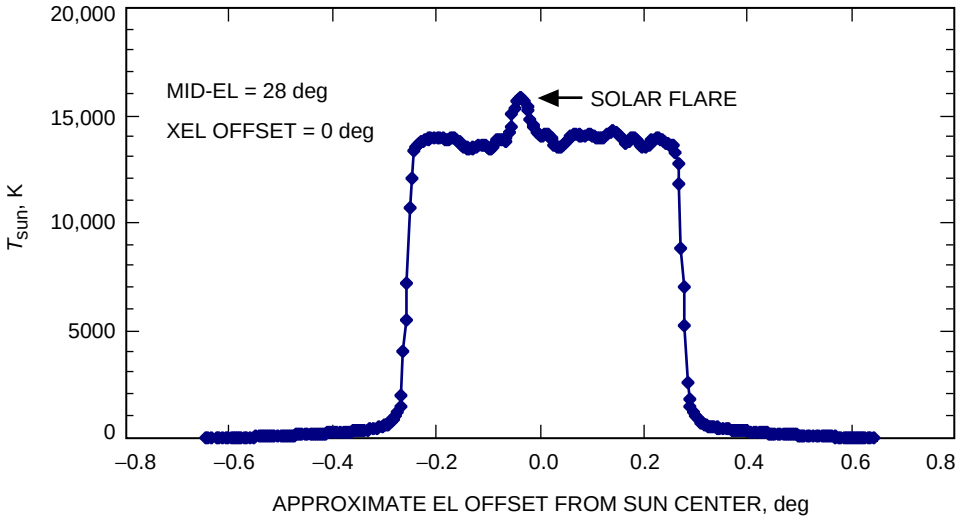

Fig. 28. DSS-13 BWG antenna, EL Sun temperature profile for XEL offset = 0 deg, 32 GHz, atmosphere removed, waveguide method, DOY 293. Corrections were made for efficiency.

number could go to zero.[5] It would be desirable to repeat these Sun measurements in a year of solar minimum. Unfortunately, since the solar cycle for solar activity is about 11 years, the solar minimum will not take place until about years 2006 to 2007.

Another possible explanation for the large difference in results obtained by the absorber and waveguide attenuator methods is that the waveguide attenuator method results might be too low due to receiver saturation. Linearity tests for the waveguide attenuator method were inconclusive because noise-diode pulses were masked out by high measurement standard deviations.

As a final comment on the experimental results, note that in Fig. 11(b) that the measured $T_{\rm sun}$ value for the absorber method was as high as 20,000 K on DOY 244. This value is considerably higher than the value of 10,530 K measured for $T_{\rm sun}$ at 31.4 GHz by Franco et al. [2]. Their measurements were made

[5] R. Woo, personal communication, Jet Propulsion Laboratory, Pasadena, California, November 2000.

in March 1981, which was also a year of maximum solar activity. However, as was shown earlier, even if measurements are done in the same year of solar maximum, on different days, the sunspot numbers can be quite different. For example, for 2000 DOY 293, Fig. 11(b) shows the average $T_{\rm sun}$ to be about 13,580 K when using the waveguide attenuator method. This DOY 293 $T_{\rm sun}$ value is much closer to the result of Franco et al. The Sun temperature measured by Franco et al. was obtained through the use of a horn whose half-power beamwidth of 6.78 deg was much wider than the 0.5-deg angular diameter of the Sun. The small horn method gives an average Sun temperature. In contrast, for the results of this article, Sun measurements were done with the use of a 34-m BWG antenna whose full half-power beamwidth of 17 mdeg was much smaller than the 0.5-deg angular diameter of the Sun. The results of this article are high-resolution point-to-point values of the Sun's temperature over the solar disk. Even though a small horn and large antenna were used to obtain $T_{\rm sun}$ values, the average measured Sun temperature values should have been closer together. The causes of large difference with the small horn result and the large antenna result are being investigated.

V. Summary and Concluding Remarks

A. Summary

The disadvantage of the absorber method is that it requires that an absorber sheet be cut to fit over the particular aperture of the receive horn to be used for the Sun experiments. The absorber sheet loss is determined by making source-temperature measurements while scanning the Moon with and without the absorber sheet and then taking the ratio of the peak temperatures. The advantage of the absorber method is that the absorber test sample can be made with the desired amount of attenuation that will make the attenuated Sun's noise power be in the linear and calibrated region of the antenna receiving system. No configuration changes in the BWG system have to be made other than placing the calibrated absorber sheet on the horn aperture. The absorber sheet loss does not have to be recalibrated if new Sun tests are continued on another day using the same receiving system.

The waveguide attenuator method is easy to use if a WR28 variable attenuator is already installed in front of the downconverter. If the WR28 attenuator is not installed, then installation could be difficult. For this method, it is required that the attenuator be adjusted until the system temperature is in the vicinity of 6500 K when the antenna points to the Sun. An inconvenience of this method is that the follow-up receiver temperature has to be remeasured after making attenuator adjustments. Then this follow-up temperature value has to be input to the computer program and the system has to be recalibrated before system temperature measurements are begun. After the tests on the Sun are completed, the attenuator has to be reset to its original setting, and the follow-up receiver temperature has to again be remeasured to ensure that the DSS-13 receiving system is restored back to its original configuration. This whole sequence has to be repeated if tests are continued on the same horn receiving system on another test date. As discussed in the article, when the waveguide attenuator method is used, with the current noise-diode instrumentation, it is not possible to know if the receiver is operating in its linear region when the antenna is pointing at the Sun. The current noise-calibration system injects a noise-diode pulse of only 16 K that is masked out due to measured Sun noise-temperature standard deviations being as large as 21 K when the antenna points at the Sun.

B. Concluding Remarks

In the future, a good experiment for checking whether the Sun temperatures, measured with the waveguide attenuator method, are in the linear region of the receiving system is to do the following. First set up the receiving system for the waveguide attenuator method configuration and measure system temperatures while doing a XEL scan through the Sun center. Then, immediately after this scan, repeat the XEL scan with the absorber sheet covering the horn aperture. If, after correcting for absorber sheet loss, the results from the two tests compare favorably, it can be concluded that the receiver was operating in the linear region for the waveguide attenuator method receiver configuration. Unfortunately this idea of performing a sequential comparison test was not thought of until too late.

If the Sun Experiment Task is continued in the future, new development work should be done to extend the receiver linear and calibrated region from the present 350 K to about 10,000 K. One way to do this is to develop new noise-calibration instrumentation that has an option to switch to a noise diode that injects about 200 K noise-diode pulses (rather than only 16 K) into the receiver. Another suggestion is to develop and use an accurately calibrated hot noise source standard of about 10,000 K if the waveguide attenuator method is the method to be adopted rather than the absorber method. The National Institute of Technology and Standards has several reports on their development of hot noise standards.

Problems that made it difficult to get better experimental data were that (1) the coordinates of the Sun center were not in the Radio Source Catalog for the DSS-13 BWG antenna, so blind pointing had to be done to find an approximate Sun center, and (2) the BWG antenna control computer crashed on two of the three test dates.

Even though the Sun data were not repeatable, the results presented in this article will be useful for studying the Sun temperature characteristics in a period of maximum solar activity. System noise-temperature data, recorded at a rate of a data point every 2 seconds, are stored into computer files called total power radiometer (TPR) files. The stored TPR data can later be used to generate expanded noise-temperature plots that have a resolution of 5 mdeg for any desired XEL region that was scanned. For example, a detailed study of the temperature profile at the outer-edge regions of the solar disk can be made. This information might be valuable to telecommunications link analysts who are interested in knowing the noise-temperature characteristics of the Sun when a spacecraft is near the edge of the solar disk [4]. To this author's knowledge, this is the first time that a large (34-m diameter) antenna was pointed at the entire solar disk to measure the Sun's noise temperature in detail at 32 GHz.

Acknowledgments

The author acknowledges the following persons for their contributions.

Goldstone DSS 13: Juan Garnica, formerly of DSS 13, made the Ka-band absorber sample and sample holder. Bob Rees, Paul Dendrenos, Lester Smith, and Gary Bury performed the Sun and Moon noise-temperature measurements at 32 GHz using the 34-m BWG Antenna.

Communications Ground Systems Section: Watt Veruttipong furnished the subreflector defocus plots for the 34-m BWG antenna at 32 GHz. He also furnished detailed E- and H-pattern data for the 34-m antenna from 0 to 180 deg used to compute theoretical measured Sun noise temperatures. Richard Cirillo, Jr., made gain measurements of the Ka-band horn and absorber at 32 GHz on the near-field range. Richard Woo provided information on sunspots.

Spacecraft Communications and Equipment Section: Bob Thomas made gain measurements of the Ku-band horn and absorber at 17 GHz on the far-field antenna range located in JPL Building 243.

Microwave and Lidar Technology Section: Steve Keihm and Al Tanner provided advanced water vapor radiometer atmospheric noise values used to compute atmospheric losses on 2000 DOY 293.

Communications Systems and Research Section: Paul Richter suggested the Sun Experiment Task and provided continued support from inception to completion. Dave Morabito provided the 32-GHz efficiency curve coefficients for the Ka-band monopulse BWG system. Steve Slobin suggested using the Moon as a strong radio source at 32 GHz for calibrating the absorber sheet.

References

[1] J. L. Linsky, "A Recalibration of the Quiet sun Millimeter Spectrum Based on the Moon as an Absolute Radiometric Standard," *Solar Physics*, vol. 28, pp. 419–424, 1973.

[2] M. M. Franco, S. D. Slobin, and C. T. Stelzried, "20.7- and 31.4-GHz Solar Disk Temperature Measurement," *The Telecommunications and Data Acquisition Progress Report 42-64, May and June 1981*, Jet Propulsion Laboratory, Pasadena, California, pp. 140–159, August 15, 1981.
http://tmo.jpl.nasa.gov/tmo/progress_report/42-64/64R.PDF

[3] T. A. Rebold, T. K. Peng, and S. D. Slobin, "X-Band Noise Temperature Near the Sun at a 34-Meter High Efficiency Antenna," *The Telecommunications and Data Acquisition Progress Report 42-93, January–March 1988*, Jet Propulsion Laboratory, Pasadena, California, pp. 247–256, May 15, 1988.
http://tmo.jpl.nasa.gov/tmo/progress_report/42-93/93V.PDF

[4] D. Morabito, S. Shambayati, S. Butman, D. Fort, and S. Finley, "The 1998 Mars Global Surveyor Solar Corona Experiment," *The Telecommunications and Mission Operations Progress Report 42-142, April–June 2000*, Jet Propulsion Laboratory, Pasadena, California, pp. 1–18, August 15, 2000.
http://tmo.jpl.nasa.gov/tmo/progress_report/42-142/142C.pdf

[5] D. A. Bathker, W. Veruttipong, T. Y. Otoshi, and P. W. Cramer, Jr., "Beam-Waveguide Antenna Performance Predictions with Comparisons to Experimental Results," *Microwave Theory and Techniques*, Special Issue (Microwaves in Space), vol. MTT-40, no. 6, pp. 1274–1285, June 1992.

[6] T. Y. Otoshi, "Determination of the Follow-up Receiver Noise-Temperature Contribution," *The Telecommunications and Mission Operations Progress Report 42-143, July–September 2000*, Jet Propulsion Laboratory, Pasadena, California, pp. 1–11, November 15, 2000.
http://tmo.jpl.nasa.gov/tmo/progress_report/42-143/143G.pdf

[7] C. T. Stelzried and M. J. Klein, "Precision DSN Radiometer Systems: Impact on Microwave Calibrations," *IEEE Proceedings*, vol. 82, no. 5, May 1995. (For discussion of mini-cals, see the Appendix, p. 784). Corrections in *Proceedings of the IEEE*, vol. 84, no. 8, p. 1187, August 1996.

[8] S. D. Slobin, T. Y. Otoshi, L. S. Alvarez, M. J. Britcliffe, S. R. Stewart, and M. M. Franco, "Efficiency Measurement Techniques for Calibration of a Prototype 34-Meter Diameter Beam-Waveguide Antenna at 8.45 and 32 GHz," *Microwave Theory and Techniques*, Special Issue (Microwaves in Space), vol. MTT-40, no. 6, pp. 1301–1309, June 1992.

[9] T. Otoshi and C. T. Stelzried, "Antenna Temperature Analysis," *Space Programs Summary 37-36*, vol. IV, Jet Propulsion Laboratory, Pasadena, California, pp. 262–267, December 31, 1965.

Appendix

Calculated Sun Noise-Temperature Profiles as Functions of XEL Scans with the 34-Meter Antenna at 32 GHz

Calculations of Sun noise temperatures as a function of XEL and EL offset angles were made through the use of a newly developed FORTRAN computer program called SUNSCAN.FOR. This program calculates antenna temperature versus antenna pointing angle looking on and off a radio source such as the Sun. Antenna temperature differs from system temperature in that it does not include the LNA and follow-up receiver contributions. The SUNSCAN program was developed by combining the features of FORTRAN programs TYO61M4 [9] and TSTSPILL.FOR.[6]

The inputs to this program are (1) the source disk noise temperature (need not be constant over the disk surface), (2) the antenna pattern of the antenna observing the source, and (3) the coordinates of the source in EL and azimuth angles. The antenna can be scanned through a stationary source as functions of antenna pointing angle in EL and XEL. The purpose of developing this program is to compute theoretical source noise-temperature profiles as a function of XEL and EL angles, source size, and the antenna patterns of the particular antenna being used for scanning through the source. Comparisons are made between the calculated and the measured source-noise temperatures. It would be of interest to see what kind of noise-temperature profile would be measured for different kinds of antenna patterns.

For the current results, the observing antenna is a 34-m antenna similar to the DSN 34-m beam-waveguide antenna. The antenna pattern of the main beam and side lobes and back lobes are shown in Fig. A-1. Only the right half of the beam is shown because it is understood that the left half is identical and symmetrical about the peak of the main beam at zero deg. Figure A-1(a) shows the pattern with the main beam and close-in lobes out to 0.5 deg, where the E- and H-plane patterns are nearly identical, and Fig. A-1(b) shows the pattern from 0.5 deg to 180 deg. The peak gain (or sometimes called directivity) of the 34-m antenna was calculated to be 80.8 dB. The antenna pattern as a function of the phi coordinate (going from 0 to 360 deg) is derived from the E- and H-patterns [9].

Table A-1 shows beam efficiency as a function at some selected antenna angles. Beam efficiency is defined as the fraction of the total power contained in the annular solid angle between the peak of the main beam out to an antenna angle theta [8]. Phi goes from 0 to 360 in this solid angle. Values of beam efficiency for the 34-m BWG antenna were obtained from the computer program SUNSCAN.FOR. Points of interest are (1) where the main beam is 44-mdeg wide and the beam efficiency is 0.871, (2) the fact that, when the first side lobe is included, the antenna beam width is 78-mdeg wide and the beam efficiency is 0.943, and (3) the fact that, when the antenna beamwidth is 500-mdeg wide, corresponding to the diameter of the Sun, the beam efficiency is about 0.9974. It will be shown by plots of the theoretical Sun scans that, when the antenna is pointed at the Sun center, the observed noise temperature is close to the product of the beam efficiency of 0.9974 times the Sun disk brightness temperature of 10,000 K. These plots of XEL are independent of the elevation angle (i.e., the same Sun plot applies whether the EL is any angle at or between 0 and 89 deg. It is assumed that the appropriate atmospheric noise temperature and cosmic background noise temperature have been removed).

---

[6] T. Y. Otoshi, "Part 1, Horizon Mask Studies with Antenna Temperature Program TSTSPILL.FOR," JPL D-15555 (internal document), Jet Propulsion Laboratory, Pasadena, California, April 16, 1997.

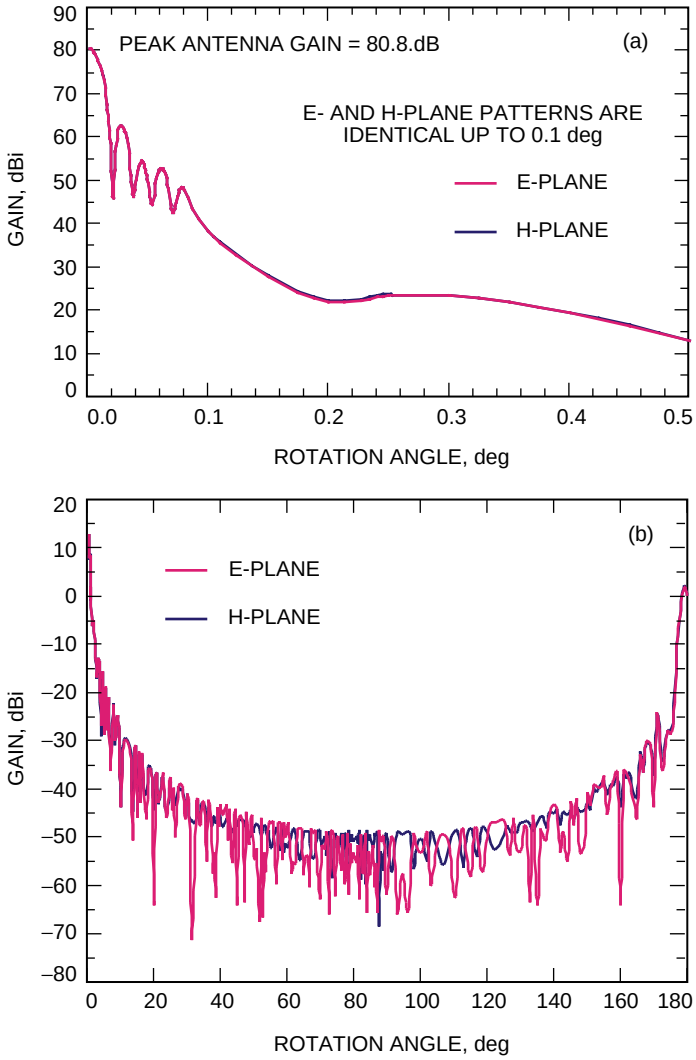

Fig. A-1. The 34-m Cassegrain antenna E- and H-plane gain patterns at 32 GHz and rotation angles of: (a) 0 to 0.5 deg and (b) 0.5 to 180 deg. Only the right-hand side of the full pattern is shown.

The Sun scans shown in Figs. A-2 through A-4 are applicable for the Sun at any elevation angle because of the relationship

$$\Delta\mathrm{XEL} = (\Delta\mathrm{Az}) \times \cos(\mathrm{EL})$$

where ΔXEL is the change in XEL angles, ΔAz is the change in azimuth angles, and EL is the elevation angle. For example, if scanning is done at a fixed but higher elevation angle, cos (EL) becomes smaller and ΔAz becomes larger (by the appropriate amount), such that the ΔXEL scans of a source will be the same at all elevation angles. This formula is built into the antenna control software.[7]

Figure A-2 shows the calculated Sun noise temperature profile when the Sun is scanned by the 34-m antenna from XEL angles from -0.5 deg to 0.5 deg for an EL offset of 0 deg. The Sun is assumed to

[7] S. Slobin, personal communication, Jet Propulsion Laboratory, Pasadena, California, February 27, 2001.

Table A-1. 34-m beam-waveguide antenna beam efficiency at 32 GHz.

Theta, deg	Full BW, deg	E-plane gain, dBi	H-plane gain, dBi	Beam efficiency	Comments[a]
0.000	0.000	80.49	80.49	0.000000	
0.002	0.004	80.45	80.45	0.018107	
0.006	0.012	79.51	79.51	0.240309	
0.010	0.020	77.18	77.18	0.558808	
0.014	0.028	72.97	72.97	0.785131	
0.018	0.036	65.08	65.08	0.864454	
0.022	0.044	45.98	45.98	0.870731	Edge MB
0.026	0.052	61.52	61.52	0.884175	
0.028	0.056	62.56	62.56	0.899246	
0.030	0.060	62.29	62.29	0.915527	
0.034	0.068	58.37	58.37	0.937799	
0.039	0.078	46.23	46.23	0.943232	Edge of SL1
0.042	0.084	52.04	52.04	0.945376	
0.046	0.092	54.42	54.42	0.952629	
0.050	0.100	51.18	51.18	0.958719	
0.054	0.108	44.52	44.52	0.960425	Edge of SL2
0.058	0.116	50.60	50.60	0.963095	
0.062	0.124	52.72	52.72	0.969727	
0.064	0.128	52.20	52.20	0.973272	
0.068	0.136	48.04	48.04	0.977677	
0.072	0.144	42.53	42.53	0.978887	Edge of SL3
0.076	0.152	47.13	47.13	0.980642	
0.080	0.160	48.25	48.25	0.983969	
0.151	0.302	27.96	27.82	0.996890	
0.251	0.502	23.58	23.57	0.997393	Edge of Sun
0.256	0.512	23.48	23.47	0.997637	
0.301	0.602	23.39	23.36	0.998143	
0.351	0.702	21.89	21.84	0.998582	
0.401	0.802	19.54	19.45	0.998873	
0.451	0.902	16.51	16.40	0.999036	
0.501	1.002	12.95	12.86	0.999115	
0.551	1.102	9.38	9.41	0.999154	
0.601	1.202	7.55	7.67	0.999183	Edge of SL4

[a] BW = beamwidth, MB = main beam, and SL = side lobe.

have a disk diameter of 0.5 deg and a constant disk noise temperature of 10,000 K at 32 GHz. Figure A-3 is an XEL plot when the 34-m antenna scans the Sun when the EL offset is 0.2 deg. Figure A-4 is a plot when the 34-m antenna scans through the Sun in the elevation direction and the XEL offset is 0 deg. The frequency for all plots is 32 GHz.

Note on the Fig. A-2 and Fig. A-4 plots that the maximum observed noise temperature at the center of the Sun is 9975 K and not 10,000 K. This is because only 99.75 percent of the antenna beam power illuminates the Sun out to its edges when the antenna points at the Sun center (see Table A-1).

The program SUNSCAN.FOR can also be used to obtain theoretical noise-temperature profiles when scanning the Sun with a reflector antenna with a smaller diameter (eg., the advanced water vapor radiometer antenna at 22.235 GHz)[8] and when scanning the Sun with a horn [2]. The program can also be used to obtain theoretical values when scanning small radio source such as those used previously for calibrating the DSN 34-m beam-waveguide antenna at 8.450 and 32 GHz [8].

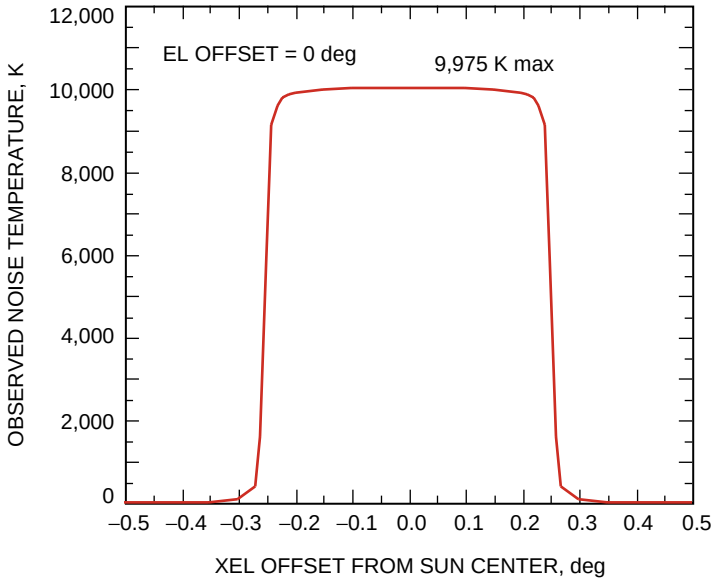

Fig. A-2. XEL scan across an ideal quiet Sun with a 34-m antenna at 32 GHz, EL offset = 0 deg. Sun disk temperature = 10,000 K. Observed noise temperatures are calculated values.

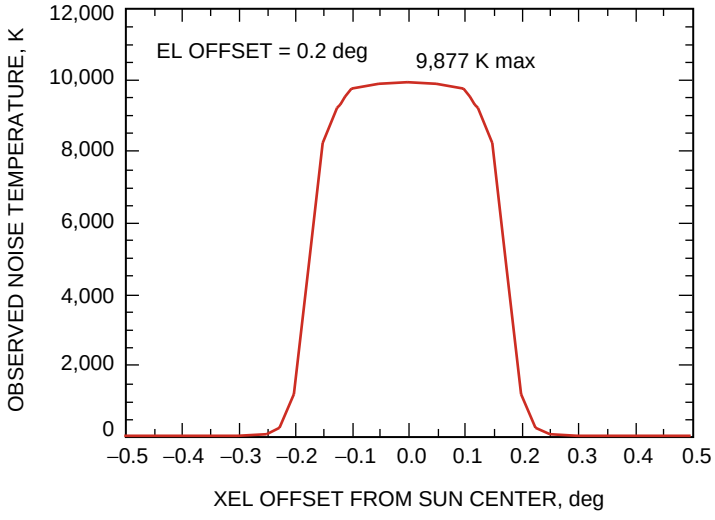

Fig. A-3. XEL scan across an ideal quiet Sun with a 34-m antenna at 32 GHz, EL offset = 0.2 deg. Sun disk temperature = 10,000 K. Observed noise temperatures are calculated values.

[8] T. Y. Otoshi, op cit.

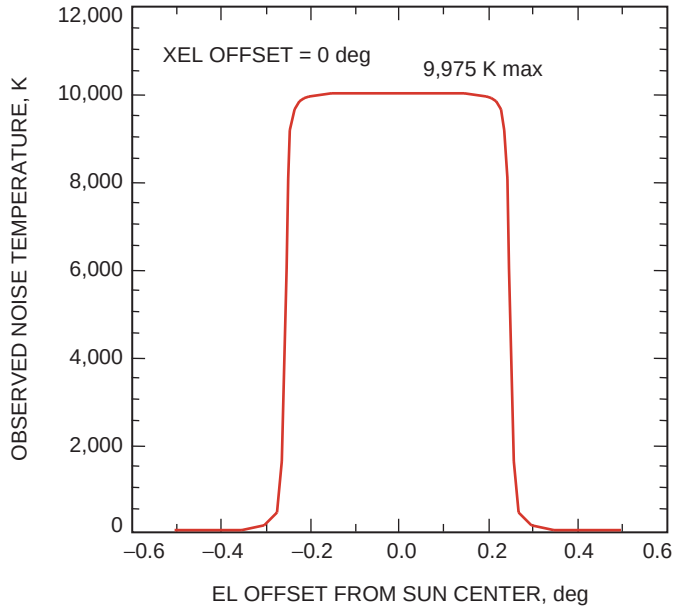

Fig. A-4. EL scan through an ideal Sun with a 34-m antenna at 32 GHz, XEL offset = 0 deg. Sun disk temperature = 10,000 K. Observed noise temperatures are calculated values.